MICROBIOLOGY

Dual therapeutic targeting of intra-articular inflammation and intracellular bacteria enhances chondroprotection in septic arthritis

Hyuk-Kwon Kwon[1], Inkyu Lee[1†], Kristin E. Yu[1], Sean V. Cahill[1], Kareme D. Alder[1], Saelim Lee[1‡], Christopher M. Dussik[1], JungHo Back[1], Jeongjoon Choi[2], Lee Song[3], Themis R. Kyriakides[4,5], Francis Y. Lee[1]*

Bacterial infections involving joints and vital organs represent a challenging clinical problem because of the two concurrent therapeutic goals of bacterial eradication and tissue preservation. In the case of septic arthritis, permanent destruction of articular cartilage by intense host inflammation is commonly seen even after successful treatment of bacterial infection. Here, we provide scientific evidence of a novel treatment modality that can protect articular cartilage and enhanced eradication of causative bacteria in septic arthritis. Locally delivered cell-penetrating antibiotics such as rifampicin effectively eradicate intracellular reservoirs of methicillin-resistant *Staphylococcus aureus* within joint cells. Furthermore, mitigation of intra-articular inflammation by targeting the NLRP3 (nucleotide-binding oligomerization domain-, leucine-rich repeat- and pyrin domain-containing 3) inflammasome protects articular cartilage from damage in a murine model of knee septic arthritis. Together, concurrent mitigation of intra-articular inflammation and local adjuvant targeting of intracellular bacteria represents a promising new therapeutic strategy for septic arthritis.

INTRODUCTION

Septic arthritis constitutes an emergent medical condition in which bacteria infect a synovial joint, which is a naturally closed compartment encased by synovial membranes and articular surfaces (*1*–*3*). Bacteria elicit intense inflammation within this closed cavity that levies sustained detrimental effects upon articular cartilage (*2*, *4*). *Staphylococcus aureus* (*S. aureus*) is the most commonly implicated pathogen in septic arthritis (*5*). Septic arthritis is often complicated by recurrent infection despite prolonged intravenous antibiotic treatment (*6*). Antibiotic resistance, particularly the rising prevalence of methicillin-resistant *S. aureus* (MRSA) infections, further complicates the treatment of septic arthritis (*7*). Internalization of *S. aureus* by host cells is one possible mechanism of recalcitrance and recurrence (*3*, *8*–*11*). Although studies concerning the eradication of intracellular bacteria have been conducted (*11*–*13*), cell-penetrating antibiotics capable of killing intracellular *S. aureus* and locally applied antibiotics have not been extensively studied as adjuvant therapies for the treatment of septic arthritis.

Although systemic antibiotic administration centers on treating the initial infection, underlying joint inflammation has long been unaddressed in septic arthritis therapies. Bacteria incite inflammatory responses characterized by the release of cytokines that sequentially amplify inflammation in tissue-resident and tissue-recruited cells within the synovial joint (*1*). The interleukin-1 (IL-1) family of cytokines is associated with innate immune responses and inflammation and mediates the propagation of inflammatory diseases such as arthritides including rheumatoid arthritis and osteoarthritis (*14*). Among the members of the IL-1 family, IL-1β is the most studied and is known to be produced by the infiltration of immune cells into joints during the pathogenesis of arthritic diseases. The maturation and release of IL-1β typically require two distinct signals: a priming signal and an activating signal (*15*). First, the stimulation of receptors by cytokine ligands such as IL-1β and tumor necrosis factor–α (TNF-α) or Toll-like receptor ligands such as pathogen-associated molecular patterns (PAMPs) and danger-associated molecular patterns (DAMPs) leads to activation of nuclear factor κ–light-chain enhancer of activated B cells. These processes lead to the expression and accumulation of the nucleotide-binding oligomerization domain-, leucine-rich repeat- and pyrin domain-containing 3 (NLRP3) inflammasome components such as NLRP3 and pro–IL-1β in the cytosol. The activating signal is triggered by local PAMPs or DAMPs including ion fluxes, reactive oxygen species generation, lysosomal destabilization, and metabolic changes, thereby promoting NLRP3 inflammasome formation and caspase-1–mediated IL-1β secretion and pyroptosis. Numerous therapeutic candidates targeting NLRP3 inflammasomes are approved or are being evaluated in clinical trials for the treatment of various diseases such as gout, cryopyrin-associated autoinflammatory syndromes, and type 2 diabetes mellitus (*15*). Nevertheless, the role of the NLRP3 inflammasome and therapeutic possibility of NLRP3 inflammasome inhibitors in combination with cell-penetrating antibiotics for the treatment of septic arthritis caused by MRSA has not been reported. Here, we sought evidence to test our hypothesis that therapeutic modulation of host inflammatory responses and intracellular MRSA eradication mitigates articular cartilage damage compared to conventional intravenous antibiotic therapy for MRSA septic arthritis.

[1]Department of Orthopaedics and Rehabilitation, Yale University School of Medicine, 800 Howard Ave., New Haven, CT 06510, USA. [2]Department of Microbial Pathogenesis, Yale School of Medicine, 295 Congress Ave., New Haven, CT 06536, USA. [3]Department of Orthopedics Surgery, Columbia University, New York, NY 10032, USA. [4]Department of Biomedical Engineering, Yale University, New Haven, CT 06520, USA. [5]Department of Pathology, Yale School of Medicine, New Haven, CT 06520, USA.
*Corresponding author. Email: francis.lee@yale.edu
†Present address: Department of Life Sciences, Chung-Ang University, Seoul, Republic of Korea.
‡Present address: College of Medicine, Dankook University, Cheonan, Republic of Korea.

RESULTS

MRSA induces intra-articular inflammation and cartilage degradation through NLRP3 pathway–mediated inflammatory processes

MRSA constitutively expressive of green fluorescent protein (GFP) was cultured on Mueller-Hinton agar plates containing oxacillin to confirm selective MRSA growth for use in subsequent experiments. To simulate human synovial joint infection, different concentrations of MRSA were intra-articularly inoculated under the patella of each mouse (Fig. 1A). Clinically, patients with septic arthritis present with erythema, warmth, stiffness, and edema of the joint (*16*) and demonstrate altered white blood cell (WBC) counts (*17*). We observed macroscopic inflammatory changes in infected murine joints including joint edema that increased with greater MRSA bioburden (Fig. 1B). WBC counts increased with higher proportions of neutrophils in the setting of MRSA infection (Fig. 1C). Synovial fluid analysis represents the gold standard of septic arthritis diagnosis and includes WBC count, Gram staining, fluid culture, and the quantification of proinflammatory cytokine expression (*18*). Synovial joint WBC counts significant increased with greater inoculated concentrations of MRSA and over time, such that light-yellow, turbid synovial fluid was isolated from infected joints after 7 days (Fig. 1D). Most WBCs reclaimed from infected synovial fluid revealed GFP-positive MRSA. We measured the viability of MRSA reclaimed from these synovial aspirates and quantified the growth of these isolates in colony-forming units (CFU), thus fulfilling Koch's germ theory (Fig. 1E). Last, synovial fluid IL-1β and IL-6 production on day 7 demonstrated a dose-response relationship with MRSA bioburden within the knee joint (Fig. 1F). These findings suggest that human septic arthritis can be reestablished in a murine knee joint model with respect to clinical signs of inflammation and cytokine production.

Transcriptomic analysis of bone marrow–derived macrophages infected with intracellular MRSA was performed using RNA sequencing (RNA-seq) and demonstrated that markers of innate inflammation such as IL-1β and IL-6 were activated in the setting of MRSA infection (Fig. 1G). Concurrent IL-1β expression and activation of innate immune receptors resulted in the up-regulation of genes associated with various inflammatory responses and diseases. In a similar fashion to the transcriptome results, increases in the expression of proinflammatory cytokines, chemokines, matrix metalloproteinases (MMPs), and induced immune responses were observed following MRSA infection of murine joints (Fig. 1H and fig. S1A). Levels of IL-1β, an intra-articular cytokine that regulates the expression of inflammatory tissue-degrading enzymes, significantly increased in the setting of MRSA infection across all time periods. We then verified NLRP3 inflammasome and inflammation in human synovial and cartilage tissues (Fig. 1, I to L). mRNA expression of proinflammatory cytokine and chemokine genes, MMPs, and pentraxin 3 (*PTX3*) was significantly higher in infected synovial tissue compared to noninfected samples (Fig. 1I and fig. S1B). MRSA strongly induced NLRP3 and IL-1β expression and activation of caspase-1 and IL-1β, although expression of apoptosis-associated speck-like protein containing a caspase activation and recruitment domain (ASC) remained unchanged (Fig. 1J). No significant changes to the intrinsic apoptosis pathway mediated by mitochondria-mediated caspase-3 signaling were observed, as measured by the expression of B cell lymphoma 2 (Bcl2), caspase-3–cleaved poly(adenosine diphosphate–ribose) polymerase 1 (PARP1), and caspase-3 activation. However, caspase-1 activation was significantly more pronounced in comparison to caspase-3, highlighting the importance of caspase-1–mediated signaling pathways in MRSA-induced septic arthritis. Chondrocytes in MRSA-infected cartilage demonstrated colocalization and higher expression of NLRP3, IL-1β, and MMP3 compared to noninfected controls (Fig. 1K). Moreover, expression of NLRP3 and IL-1β increased and were coexpressed and colocalized in MRSA-infected synovial tissues (Fig. 1K and fig. S2). IL-1β production was reduced by OLT1177 (OLT), an approved NLRP inflammasome inhibitor with demonstrated safety in human clinical trials (*19*, *20*), without significant cytotoxic effects in heat-killed (HK)–MRSA–primed synovial cells stimulated with adenosine triphosphate (ATP) (Fig. 1L). Under equivalent conditions, OLT showed a slight inhibitory effect on IL-6 production. Therefore, MRSA-induced septic arthritis generates inflammatory responses involving the NLRP3 inflammasome in cartilage and subchondral bone.

Systemic antibiotic treatment reduces bacterial burden but intracellular bacteria and inflammation persist

We investigated whether systemic treatment with vancomycin, an antibiotic commonly used in the treatment of septic arthritis (*21*, *22*), effectively attenuates both infection and inflammation (Fig. 2A). Systemic antibiotic treatment reduced knee joint edema compared with the untreated MRSA group, although no significant differences in WBC counts were observed (Fig. 2, B and C). Systemic antibiotic treatment markedly reduced the number of inflammatory cells and MRSA in synovial fluid samples compared with the untreated MRSA group (Fig. 2D). Nevertheless, systemic antibiotic treatment did not reduce the concentration of intra-articular cytokines such as IL-1β and IL-6 in infected knee joints (Fig. 2E), suggesting persistent inflammation. Likewise, systemic antibiotic treatment did not significantly suppress NLRP3 expression, caspase-1 activation (22 kDa), and IL-1β maturation (17 kDa) in synovial fluid cells following MRSA infection (Fig. 2F). Within synovial tissues, MRSA induced the expression of NLRP3, IL-1β (31 kDa), MMP3, and cathepsin K, the activation of caspase-1 (12 kDa), and the maturation of IL-1β (17 kDa) and gasdermin D (GSDMD; 32 kDa); however, systemic antibiotic treatment had no effect on the levels of these inflammatory proteins (Fig. 2G). Similar to our findings in human synovial tissues, caspase-1 activation by MRSA was significantly higher than that of caspase-3 activation (19 kDa). No significant difference was observed in the levels of PARP1 (89 kDa) and GSDME (32 kDa), proteins cleaved by caspase-3, between groups.

On quantitative histopathological analysis, the infiltration of immune cells into the synovial cavity and inflammation scores increased with MRSA infection (Fig. 2H). Cartilage thickness and chondrocyte populations in articular cartilage were reduced in the setting of MRSA infection, which resulted in higher osteoarthritis research society international (OARSI) scores (Fig. 2H). MRSA increased the expression, coexpression, and colocalization of NLRP3, IL-1β, and MMP3 in synovial cells and articular chondrocytes (Fig. 2H and fig. S3A). While systemic antibiotic treatment resulted in lower inflammation and OARSI scores in MRSA infected mice, the number of chondrocytes present in articular cartilage and the size of osteophytes formed did not change significantly. Moreover, systemic antibiotic treatment did not significantly alter expression of NLRP3, IL-1β, and MMP3, although these factors were still coexpressed and colocalized to the chondrocytes of knee articular cartilage. We also found that inflammatory cells expanded into the tibial and femoral subchondral regions with the spread of MRSA

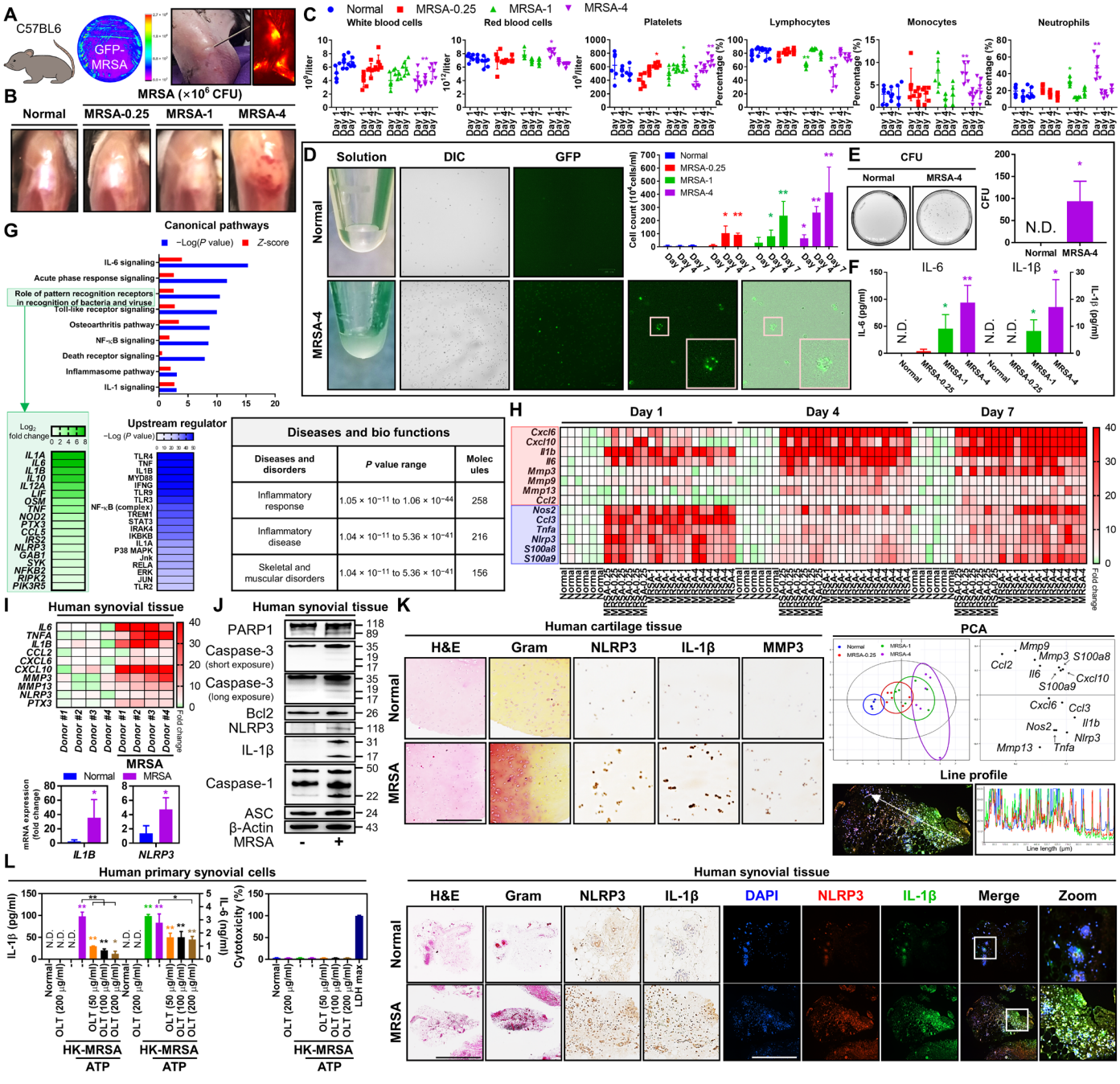

Fig. 1. MRSA-induced septic arthritis results in inflammation, cartilage degradation, and NLRP3 inflammasome activation in human and murine knee joint tissue. (**A**) C57BL/6 mice were intra-articularly injected with Dulbecco's phosphate-buffered saline (DPBS), GFP-MRSA 0.25×10^6 colony-forming units (CFU) (MRSA-0.25), GFP-MRSA 1×10^6 CFU (MRSA-1), and GFP-MRSA 4×10^6 CFU (MRSA-4) ($n = 3$ to 6 per group). (**B**) Representative knee images at 7 days. (**C**) Blood was collected at 1, 4, and 7 days for complete blood count (CBC) quantification. (**D**) MRSA were detected in synovial fluid and through differential interference contrast (DIC) as well as GFP labeling and (**E**) MRSA growth was quantified. (**F**) Synovial IL-6 and IL-1β expression was measured. (**G**) Whole-genome transcriptomic profiling of MRSA-infected bone marrow–derived macrophages was performed. Upstream regulator is indicative of the transcriptional regulators driving the observed gene expression changes. (**H**) Synovial mRNA expression was analyzed by principal components analysis (PCA) (fig. S1A). (**I** to **L**) Human synovium and cartilage were incubated with MRSA-4 for 24 hours ($n = 4$ each). (I) mRNA expression was examined (fig. S1B). (J) PARP1, caspase-3, Bcl2, NLRP3, IL-1β, caspase-1, ASC, and β-actin expression was quantified using β-actin as a control. (K) Tissue sections were visualized with hematoxylin and eosin (H&E) and Gram stains, and NLRP3, IL-1β, and MMP3 expression was detected. Colocalization of NLRP3 and IL-1β was confirmed by line profile analysis (fig. S2). (L) IL-1β, IL-6, and cytotoxicity levels in HK-MRSA–primed, ATP-stimulated synovial cells after OLT treatment. Error bars represent means ± SD. One-way analysis of variance (ANOVA) with Tukey's post hoc analysis was performed (*$P < 0.05$ or **$P < 0.01$; N.D., not detected; scale bar, 1000 μm). DAPI, 4′,6-diamidino-2-phenylindole. Photo credit: Hyuk-Kwon Kwon, Yale University.

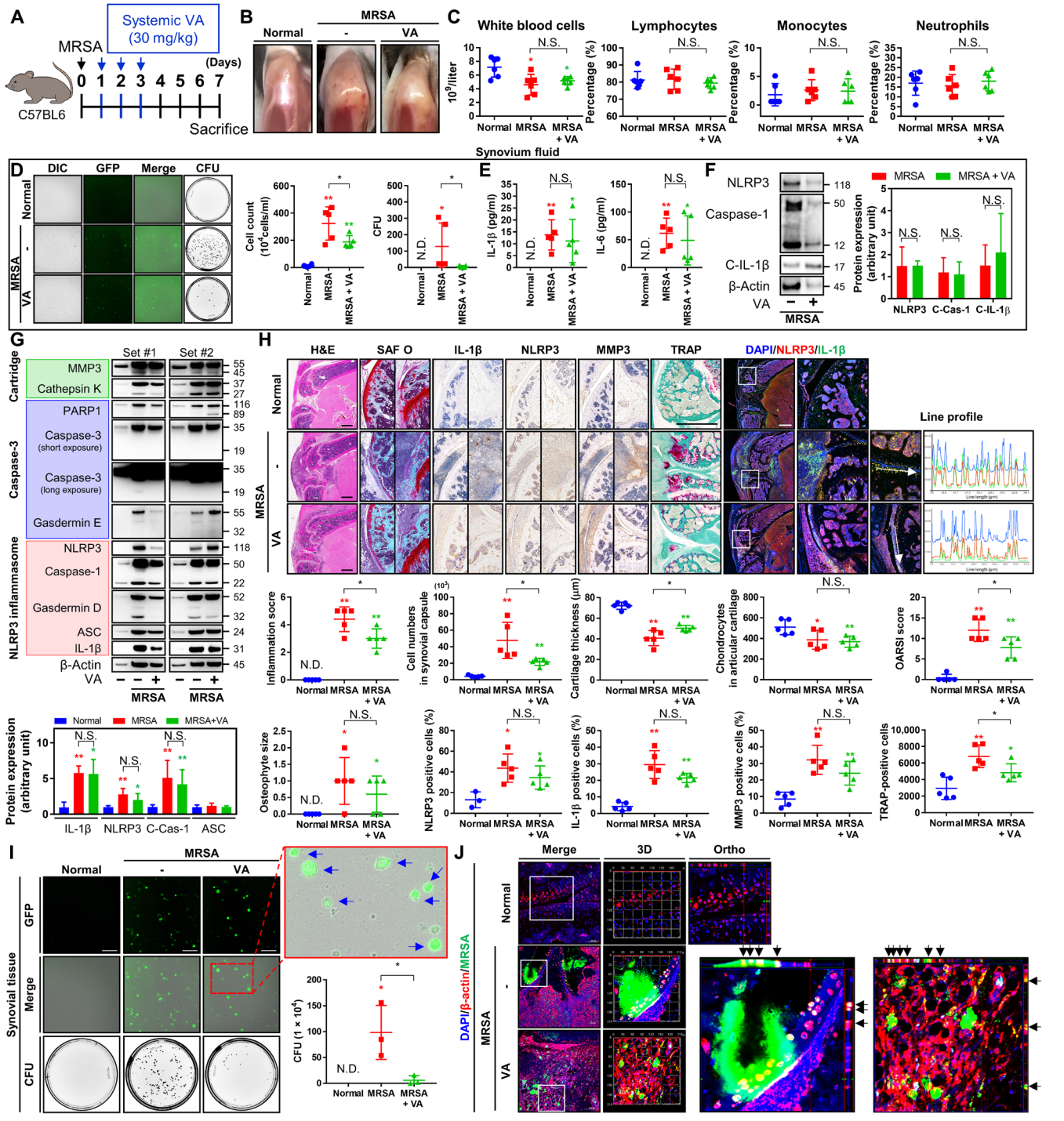

Fig. 2. Treatment with vancomycin is effective for septic arthritis caused by MRSA, but MRSA persists intracellularly and induces a proinflammatory state. (**A**) C57BL/6 mice were intra-articularly injected with DPBS or MRSA (4×10^6 CFU). One day after infection, vancomycin (VA; 30 mg/kg) was subcutaneously injected for 3 days ($n = 3$ to 5 per group). (**B**) Representative images of knees. (**C**) Blood was collected, and CBCs were obtained. (**D**) Synovial cells and GFP-labeled MRSA CFU were quantified. (**E**) Synovial IL-1β and IL-6 concentrations were quantified with or without systemic vancomycin. (**F**) Synovial fluid NLRP3, caspase-1, C-IL-1β, and β-actin expression was measured using β-actin as a loading control. (**G**) Synovial MMP3, cathepsin K, PARP1, caspase-3, GSDME, NLRP3, caspase-1, GSDMD, ASC, IL-1β, and β-actin expression was measured with a β-actin control. (**H**) Tissue sections were stained with H&E, safranin O (SAF O), and TRAP. The percentage of NLRP3-, IL-1β–, and MMP3-positive cells were quantified, and TRAP-positive cells were counted (scale bar, 1000 μm) (fig. S3A). Coexpression and colocalization of NLRP3 and IL-1β were confirmed by line profile analysis (scale bar, 1000 μm) (fig. S3B). (**I**) MRSA CFU quantification from single synovial tissue cells. The blue arrow indicates intracellular MRSA (scale bar, 100 μm). (**J**) Intracellular and extracellular MRSA were measured by multiplex immunohistochemistry and confirmed using three-dimensional (3D) and orthogonal analyses (fig. S4). Error bars show means ± SD. One- or two-way ANOVA with Tukey's post hoc analysis was used (*$P < 0.05$ or **$P < 0.01$; N.S., not significant). Photo credit: Photographer name: Hyuk-Kwon Kwon. Photographer institution: Yale University.

infection; large areas of osteolysis and reactive peripheral bone (involucrum) formation were observed in these regions. Systemic antibiotic treatment limited the spread of immune cells to these areas, as well as involucrum formation, although lytic lesions were still observed. The number of cells that stained positive for tartrate-resistant acid phosphatase (TRAP), which is indicative of osteoclasts, increased in the setting of MRSA infection (Fig. 2H and fig. S3B). High levels of TRAP were also detected in lytic lesions affecting articular cartilage. Systemic antibiotic treatment reduced the number of positively staining TRAP cells in the setting of MRSA infection, although these levels remained significantly higher than normal, suggesting that antibiotic treatment alone may not fully curb osteoclastogenesis. Numerous cells infested with GFP-positive MRSA were identified from harvested synovial tissue samples, indicating that MRSA can persist within synovial tissues and inside host cells following systemic antibiotic treatment (Fig. 2I). This was also demonstrated by high levels of intracellular GFP positivity in cartilage matrix and articular chondrocytes (Fig. 2J and fig. S4). Moreover, the human chondrocyte cell line C28/I2 showed increased intracellular MRSA levels over time following infection (fig. S5 and movie S1). These findings demonstrate the failure of current systemic antibiotic treatments to control for intracellular infection and persistent inflammation in bacterial synovial joint infection, thus necessitating new therapeutic strategies.

Antibiotic-treated bacteria continue to cause intra-articular inflammation in synovial joints

Although systemic antibiotics can mitigate the extent of bacterial infection, inflammation persists intra-articularly. MRSA susceptible to vancomycin was treated with different concentrations of vancomycin (ranging from 0.625 to 20 mg/ml) to establish bactericidal dose-response curves and create a vancomycin-treated (VT)–MRSA strain using 20 mg/ml concentration of vancomycin. Antibiotic-treated bacterial samples were then incubated on an agar plate with or without oxacillin (Fig. 3A). All VT-MRSA groups failed to grow in the presence of oxacillin (Fig. 3B). On plates without oxacillin, MRSA treated with 10 to 20 mg/ml concentration of vancomycin did not generate new colonies, while MRSA treated with 0.625 to 5 mg/ml concentration of vancomycin did. Upon intra-articular injection of MRSA, HK-MRSA, and VT-MRSA into murine knee joints (Fig. 3C), VT-MRSA induced mildly visible inflammatory changes (Fig. 3D). VT-MRSA and HK-MRSA both increased myeloperoxidase (MPO) activity on MPO fluorescent imaging (Fig. 3D). After 7 days of treatment, no significant differences in systemic inflammation were observed between the HK-MRSA and VT-MRSA on the basis of complete blood count (CBC) results (Fig. 3E). Within 1 day of intra-articular inoculation, infiltration of inflammatory cells into the synovial fluid increased in all three groups (Fig. 3F). These immune cells that infiltrated the synovial space in the setting of untreated MRSA infection intracellularly demonstrated GFP fluorescence. This observation was first observed within 24 hours of infection, persisted over the first 7 days, and resulted in the significant plated growth of MRSA isolated from the intracellular compartment. In addition, lower immune cell infiltration of the synovial space and a lack of intracellular GFP fluorescence were observed with HK-MRSA, but not VT-MRSA, in the presence of which immune cell infiltration into the joint space comparable to the untreated MRSA condition was observed. Moreover, a small number of intracellularly GFP-positive cells and low CFU counts (2 to 9 CFU) of MRSA obtained from the intracellular compartment were observed in approximately 50% of cases. Together, these findings suggest that while the HK condition resulted in fully inactivated MRSA, which elicits a less intense immune response and the inability of the bacteria to penetrate intracellularly, vancomycin treatment does not fully attenuate MRSA's pathogenicity, such that intra-articular immune cell infiltration persists. In addition, MRSA seems to retain its ability to enter the intracellular compartment under the VT condition, despite the extracellular actions of vancomycin upon the bacteria, resulting in a reservoir for continued and/or future infection and inflammation.

Inflammatory profiles were generated from serum and synovial fluid samples (Fig. 3G and fig. S6). The expression of clusters of cytokines increased in mice infected with live MRSA and VT-MRSA relative to the control and HK-MRSA groups. In both serum and synovial fluid, live MRSA induced the production of proinflammatory factors such as IL-1α, IL-6, TNF-α, CCL5, and CXCL9 within 7 days of infection. The production of IL-1β, CXCL1, and CXCL10 significantly increased only in synovial isolates. Cytokine levels were significantly higher in joint aspirates than in serum and thus represent intra-articular inflammation. While serum cytokine expression did not significantly change in the HK-MRSA and VT-MRSA groups within 7 days, synovial fluid levels of IL-1β, IL-6, CCL5, CXCL1, CXCL10, and macrophage colony-stimulating factor (M-CSF) were significantly higher in the VT-MRSA group than the HK-MRSA group. Inflammation and OARSI scores increased in the live MRSA, VT-MRSA, and HK-MRSA groups in descending order of magnitude (Fig. 3H). The percentage of IL-1β- and MMP3-expressing cells increased in the MRSA and VT-MRSA groups relative to the control. Together, these findings suggest that antibiotic-treated and even dead (HK) bacteria continue to induce joint inflammation that contributes to sustained cartilage damage, such that inflammation-mitigating therapies in conjunction with more effective antibiotic treatments are necessary to facilitate chondroprotection in septic arthritis.

Local delivery of cell-penetrating antibiotics kills intracellular bacteria that survive systemic antibiotic treatment

Clinically, vancomycin is commonly prescribed to treat MRSA infections but is incapable of penetrating eukaryotic plasma membranes (*12*). However, lipophilic antibiotics such as rifampin are able to enter eukaryotic cells and biofilms with demonstrated bactericidal activity in both domains. Thus, we hypothesized that rifampin would be an adjunctive antibiotic to eliminate intracellular MRSA. Dose-dependent increases in the size of MRSA inhibition zones were observed with combinatorial vancomycin and rifampin treatment compared with vancomycin treatment alone (Fig. 4, A and B). After identifying an effective dose of rifampin, we devised site-specific local delivery constructs using biodegradable hydrogels because of their common use, low in vivo toxicity, and multimodal applications for drug delivery (*23*). Different hydrogel percentages of thiol-modified hyaluronan with a thiol-reactive polyethylene glycol diacrylate crosslinker (0.5 to 2%) were mixed with rifampin to assess the release kinetics of rifampin-loaded hydrogels (Fig. 4C). This rifampin release profile was dependent on hydrogel composition; higher concentrations more slowly released rifampin than less concentrated hydrogels. In addition, we verified the MRSA-killing capacity of rifampin-loaded hydrogels, which reduced MRSA bioburden up to 7 days after incubation (Fig. 4D). The bactericidal effects of rifampin-loaded hydrogels on intracellular MRSA infection were assessed

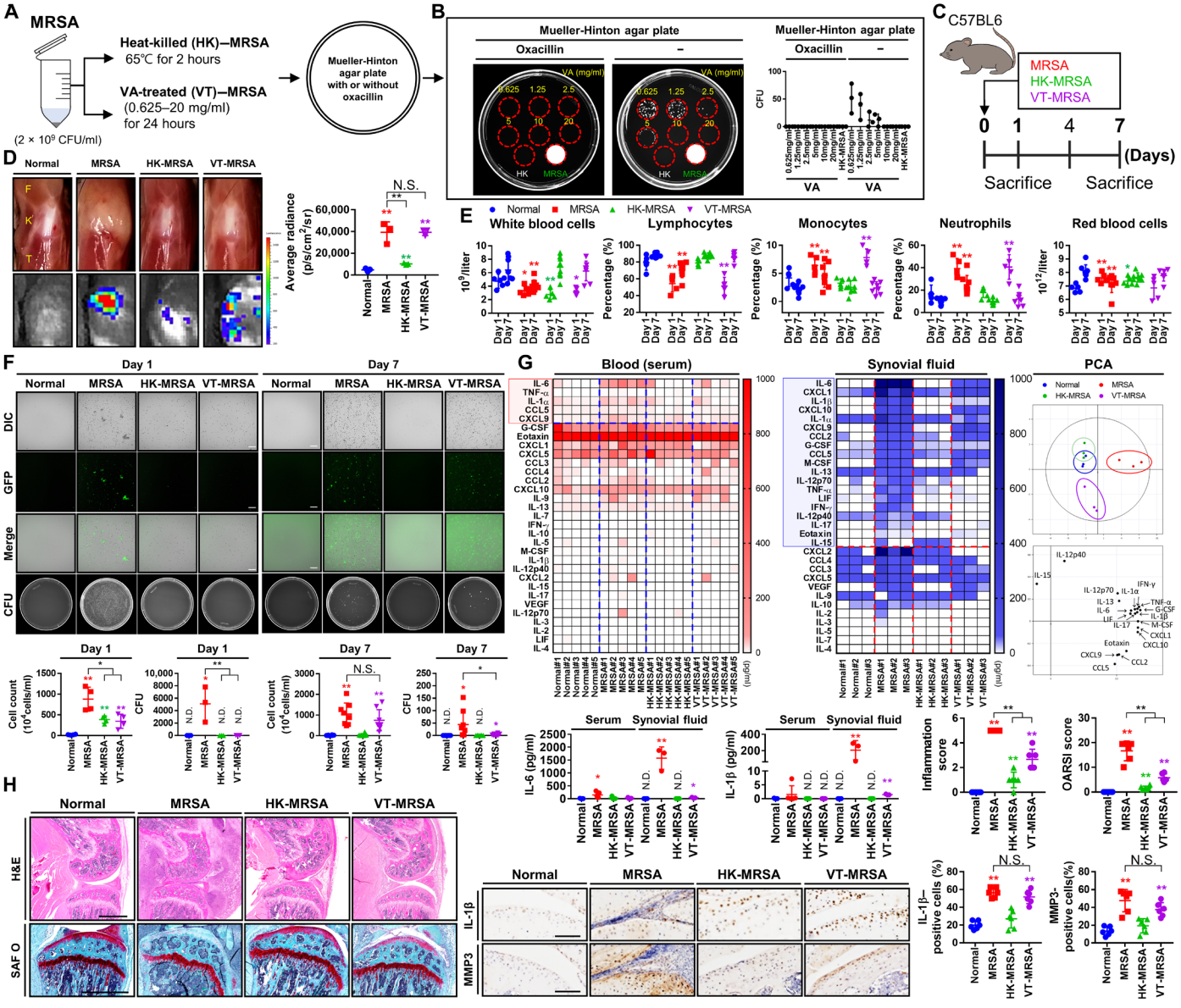

Fig. 3. MRSA directly exposed to a high dose of vancomycin allows for the recurrence of septic arthritis as evidenced by MRSA regrowth, inflammation, and cartilage damage. (**A**) MRSA (2×10^9 CFU/ml) was treated with different concentrations of vancomycin (0.625 to 20 mg/ml) for 24 hours, yielding VT-MRSA, or incubated at 65°C for 2 hours, yielding HK-MRSA. (**B**) VT-MRSA and HK-MRSA samples were seeded on plates containing either oxacillin or vehicle and incubated. MRSA was used as a positive control. The histogram presents the number of CFU from each group. (**C**) C57BL/6 mice were intra-articularly injected under the patella with DPBS (normal), MRSA (2×10^7 CFU), HK-MRSA, and VT-MRSA (20 mg/ml) ($n = 3$ to 8 per group). (**D**) Gross images of knee joints with correlative heatmaps of MPO activity within the knee joint. (**E**) Blood was collected, and CBCs were measured. (**F**) Synovial fluid cell number was measured, and levels of GFP-positive MRSA were observed in synovium cells. MRSA bioburden was quantified in CFU. (**G**) The serum and synovial inflammatory profiles of septic joints were analyzed. The red and blue boxes highlight factors that underwent significant change in the setting of infection. The synovial inflammatory profiles of septic joints were analyzed by PCA. See fig. S6 for changes in individual cytokines, chemokines, and other factors. (**H**) Paraffin-embedded tissue sections were stained with H&E and SAF O, from which inflammation and OARSI scores were calculated (scale bar, 1000 μm). NLRP3, IL-1β, and MMP3 expression was detected, and the percentages of NLRP3-, IL-1β–, MMP3-positive cells were quantified (scale bar, 100 μm). One- or two-way ANOVA with Tukey's post hoc analysis was used (*$P < 0.05$ or **$P < 0.01$). Photo credit: Photographer name: Hyuk-Kwon Kwon. Photographer institution: Yale University.

in vitro by infecting murine macrophage cells (RAW264.7) with MRSA, after which an increase in intracellular MRSA concentrations and immune response were observed over time (Fig. 4, E to H, and fig. S7). Extracellular MRSA was eradicated, simulating the clinical scenario of intracellular MRSA infection. Intracellular MRSA concentrations plateaued 2 hours after murine macrophage infection, and these intracellular MRSA remained viable in the presence of vancomycin (Fig. 4I). By contrast, rifampin effectively rendered intracellular MRSA nonviable. In MRSA-infected human synovial tissues, rifampin-loaded hydrogels effectively lowered intracellular MRSA levels. By contrast, no significant differences in MRSA bioburden were observed with vancomycin hydrogel treatment alone (Fig. 4J).

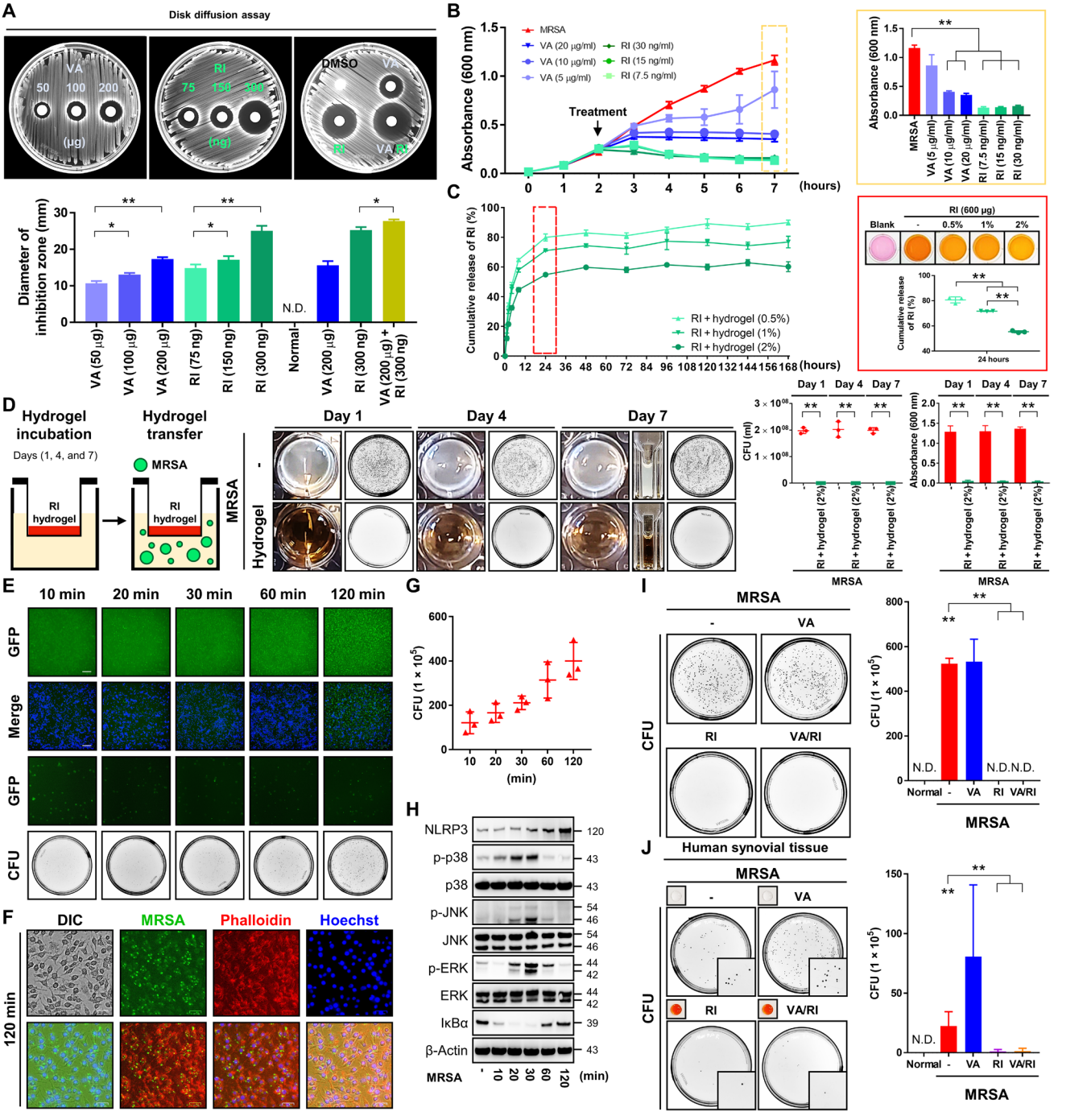

Fig. 4. Rifampin-containing hydrogels are effective in removing intracellular MRSA. (**A**) Disk fusion assays using vancomycin (20 to 200 μg), rifampin (RI; 75 to 300 ng), and vancomycin (200 μg) and rifampin (300 ng). Inhibition zone diameters were measured. DMSO, dimethyl sulfoxide. (**B**) MRSA (4×10^6 CFU) was seeded and grown for 2 hours and then treated with vancomycin (5 to 20 μg/ml) and rifampin (7.5 to 30 ng/ml). Absorbance levels are shown. (**C**) The release efficiency of rifampin (600 μg) from hydrogel (0.5 to 2%) was measured as cumulative rifampin release over time. (**D**) Two percent rifampin (600 μg) hydrogel was added in polyester (PET) track-etched membrane inserts and then transferred to lysogeny broth media containing 4×10^6 CFU MRSA after 1, 4, and 7 days. MRSA growth was measured via absorbance and CFU. (**E**) MRSA (4×10^6 CFU) was cocultured with RAW264.7 cells for 10 to 120 min, after which intracellular fluorescence was measured (fig. S7A) (scale bar, 100 μm). (**F**) Cells were stained with Phalloidin and Hoechst 120 min after infection (scale bar, 27 μm). (**G**) MRSA bioburden in this cellular suspension was counted (fig. S7B). (**H**) NLRP3, p38, c-Jun N-terminal kinase (JNK), extracellular signal–regulated kinase (ERK), inhibitor of nuclear factor κBα (IκBα), and β-actin expression was measured using β-actin as a control. (**I**) MRSA-infected cells were treated with vancomycin (300 μg/ml) and/or rifampin (60 μg/ml) 120 min after infection. Intracellular MRSA was quantified. (**J**) Human synovium was infected with MRSA (4×10^6 CFU) for 4 hours and then treated with vancomycin-loaded (300 μg/ml) and/or rifampin-loaded (60 μg/ml) hydrogel. Intracellular MRSA was quantified. Error bars show means ± SD. One- or two-way ANOVA with Tukey's post hoc analysis was performed (*$P < 0.05$ and **$P < 0.01$). Photo credit: Photographer name: Hyuk-Kwon Kwon. Photographer institution: Yale University.

In an in vivo model, local treatment of rifampin reduced the number of CFU in synovial fluid, which alleviated lameness scores (fig. S8). Together, these findings suggest that adjuvant rifampin-loaded hydrogel therapy is effective against recalcitrant MRSA infection following systemic antibiotic treatments. Moreover, the hydrogel-based local antibiotic adjuvant therapy described herein precludes systemic antibiotic toxicity.

Adjuvant inflammasome inhibitor and cell-penetrating antibiotic therapy promotes chondroprotection in septic arthritis

We hypothesized that dual attenuation of proinflammatory pathways mediated by the NLRP3 inflammasome and destruction of intracellular bacteria would protect chondrocytes in bacterial septic arthritis. Mice were intra-articularly treated with OLT and rifampin after systemic vancomycin treatment (Fig. 5A). Systemic vancomycin treatment alone did not significantly attenuate gross signs of septic arthritis compared to the untreated mice (Fig. 5B). Combined OLT with rifampin therapy markedly reduced knee edema relative to other infected groups. Combination treatment normalized infection-induced leukocytosis to near-normal levels (Fig. 5C). Results of serum inflammatory profiles were not changed, with the exception of eotaxin and CXCL5 (Fig. 5D and fig. S9). Infection-induced increases in immune cell infiltration into synovial fluid were markedly reduced after combination treatment (Fig. 5E). Moreover, lower MRSA CFU counts were observed following rifampin treatment but were unchanged in the systemic VT group relative to the untreated control. The intra-articular inflammation elicited by MRSA infection was significantly greater than serum levels representative of the systemic inflammatory response (Fig. 5F and fig. S10). Combination treatment more effectively normalized intracellular cytokine expression than the single-drug condition.

Following these inflammation-based experiments, joint architecture in the setting of infection and immune-modulating treatments was investigated via microcomputed tomography (micro-CT). Three-dimensional (3D) images revealed significant erosions in cortical and cancellous bone in the distal femoral and proximal subchondral tibiae of MRSA-infected mice (Fig. 6A). The bone volume/total volume (BV/TV) and tissue mineral density (TMD) of cortical and cancellous bone in the femora and tibiae were lower in the setting of MRSA infection. Vancomycin treatment alone failed to ameliorate MRSA-induced changes in BV/TV that were most preserved with combination treatment. Involucrum, a sign of reactive bone formation during the subacute or chronic phases of infection, in the femora and tibiae increased with MRSA infection (fig. S11). Involucrum formation occurred in 75 and 50% treated solely with OLT or rifampin, respectively. By contrast, involucrum generation was not detected in mice that received combined OLT and rifampin therapy. Similar trends were observed with respect to BV/TV and connectivity density (conn-dens.) analyses. Hematoxylin and eosin (H&E) and safranin O (SAF O) staining demonstrated that MRSA-induced inflammation scores, synovial hyperplasia, OARSI scores, reactive bone size, cartilage degradation, bone erosion, and bone formation did not meaningfully improve with systemic vancomycin treatment (Fig. 6B). These parameters improved with combination treatment, highlighting the joint preserving effects of cell-penetrating antibiotic and inflammasome inhibitor treatment in the setting of bacterial synovial joint infection. In addition, OLT and rifampin combination therapy improved lameness scores that were increased by MRSA infection.

DISCUSSION

Here, we demonstrate proof that our therapeutic strategy composed of inflammasome attenuation and cell-penetrating antibiotics eradicates intracellular MRSA and curbs the inflammatory degradation of cartilage (Fig. 6C).

S. aureus can be internalized into host phagocytic cells (*24*, *25*) and nonphagocytic cells (*26*, *27*) that then serve as reservoirs for recurrent osteomyelitis and septic arthritis (*28*, *29*). Our findings recapitulate that MRSA is capable of intracellularly infecting immune and synovial cells. We demonstrate that systemic vancomycin treatment is effective in decreasing the overall MRSA burden in septic arthritis but incapable of eradicating intracellular MRSA infestation within immune cells and joint tissue. This phenomenon likely contributes to the recalcitrant nature of septic joint infections. Before this study, it was unknown whether *S. aureus* could directly infect chondrocytes in vivo. This study demonstrates that MRSA can penetrate chondrocytes through degraded cartilage clefts. Rifampin was chosen because of its ability to strongly penetrate eukaryotic cell plasma membranes secondary to its strong lipophilicity (*12*). We determined that cell-penetrating antibiotics are effective against intracellular infection, in addition to the systemic administration of vancomycin that represents the standard of care for septic arthritis. Numerous in vitro and in vivo studies have demonstrated that combination therapy with rifampin and vancomycin is efficacious in the treatment of *S. aureus* infections, including MRSA (*30*). Local rifampin delivery was pursued to increase local concentrations of the agent and limit its systemic side effects. Local administration of rifampin-loaded hydrogels was indeed an effective adjuvant antimicrobial therapy in addition to systemic vancomycin treatment in reducing intracellular MRSA counts in host cells and tissues. Similar to the high false-negative rate of synovial fluid cultures observed clinically (*31*), synovial fluid isolates yielded no discernible bacterial growth following systemic antibiotic treatments. Joint inflammation and infection persisted because of the recurrence of infection from bacteria within the intracellular compartment.

Septic arthritis induces the generation of inflammatory cytokines within synovial fluid that increases the expression of bone-resorptive and cartilage-degrading proteases such as MMPs and cysteine (*1*, *4*). In our study, the overall production of various inflammatory factors was increased in the setting of MRSA infection, and joint inflammation was shown to be more severely produced than systemic inflammation. Among the inflammatory factors that were up-regulated in synovial fluid in the presence of MRSA, IL-1β, IL-6, and TNF-α expression increased to the greatest extent in the MRSA and VT-MRSA groups. IL-1β—whose activation is dependent on the formation of the NLRP3 inflammasome—is one of the key mediators of articular cartilage degradation in rheumatic diseases (*14*). However, the effectiveness of therapeutic agents targeting the NLRP3 inflammasome has not been sufficiently studied in conditions such as septic arthritis. In our study, both human and murine infected synovial and cartilage tissue demonstrated increased maturation of IL-1β, as mediated by activation of caspase-1. This process has been shown to induce pyroptosis, as opposed to caspase-3–mediated apoptosis. However, despite antibiotic therapy, significant differences in NLRP3-mediated IL-1β production were not observed or were changes in the expression of various synovial inflammatory factors. Direct injection of the NLRP3 inflammasome inhibitor OLT into the knee joint in conjunction with rifampin therapy reduced inflammation and demonstrated chondroprotective effects. Increases in NLRP3

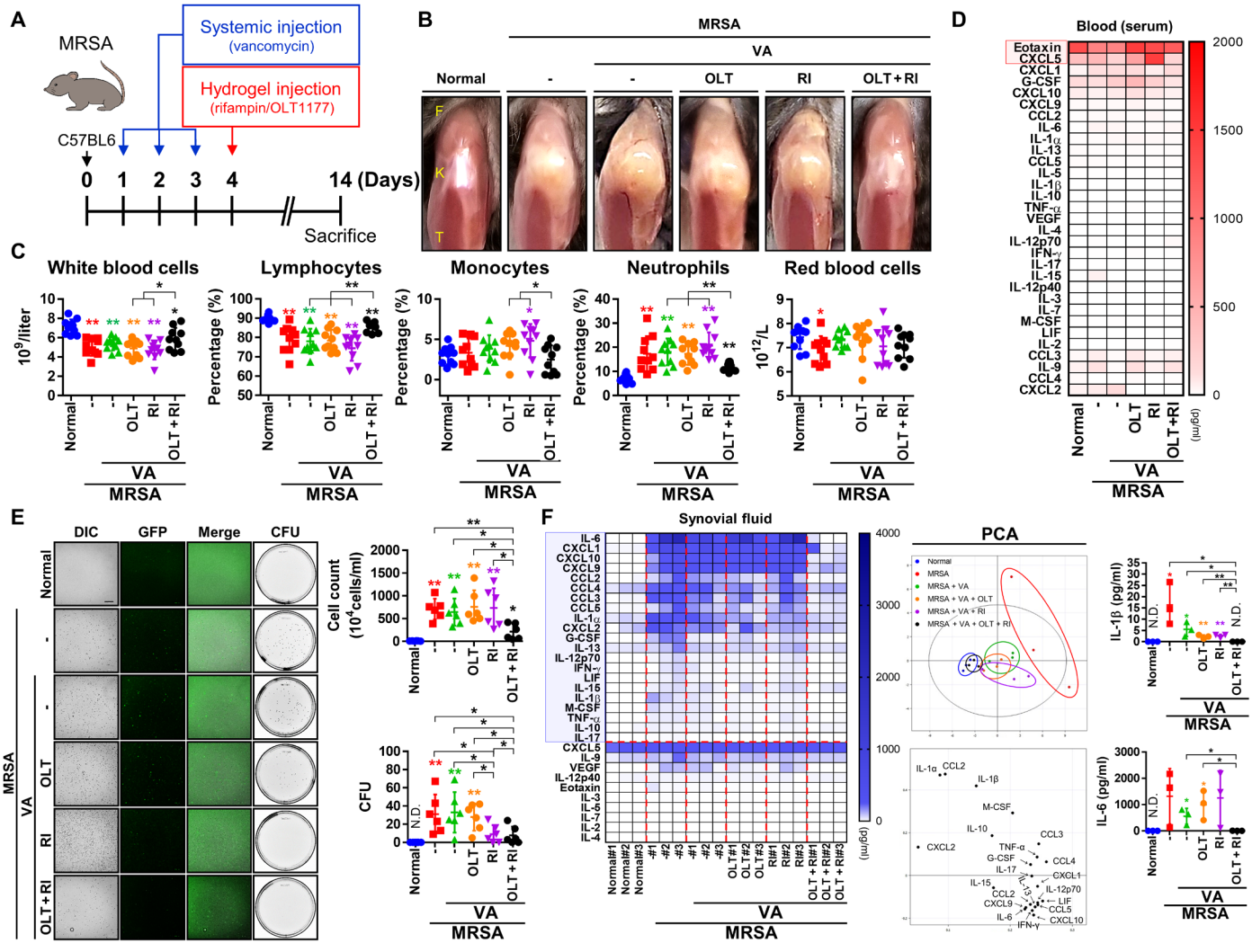

Fig. 5. Local treatment with hydrogels containing rifampin and a NLRP3 inflammasome inhibitor mitigates MRSA-induced inflammation. (**A**) C57BL/6 mice were intra-articularly injected under the patella with DPBS (normal) and MRSA (4×10^6 CFU). One day after infection, vancomycin (30 mg/kg) was administered for 3 days, after which a hydrogel (2%) containing OLT (200 μg per joint), rifampin (120 μg per joint), and OLT (200 μg per joint) + rifampin (120 μg per joint) ($n = 3$ to 10 per group) was injected intra-articularly under the patella. (**B**) Representative images of knee joints. (**C**) Blood was collected, and CBCs were measured. (**D**) The serum inflammatory profiles of septic joints were analyzed by PCA. The red box highlights factors that underwent significant change in the setting of infection. See fig. S9 for individual cytokines, chemokines, and other factors changes. (**E**) Synovial fluid cellularity was quantified, after which the presence of GFP-positive MRSA within the synovial cells was detected (scale bar, 100 μm). MRSA bioburden was quantified in CFU. (**F**) The synovial inflammatory profiles of septic joints were analyzed by PCA. The blue box highlights factors that underwent significant change in the setting of infection. See fig. S10 for individual cytokines, chemokines, and other factors changes. Error bars show means ± SD with individual data points. One- or two-way ANOVA with Tukey's post hoc analysis was performed (*$P < 0.05$ or **$P < 0.01$). Photo credit: Photographer name: Hyuk-Kwon Kwon. Photographer institution: Yale University.

inflammasome-mediated caspase-1 activation and IL-1β production are associated with persistent intra-articular inflammation and greater cartilage damage. Adjuvant therapy inclusive of anti-inflammatory medications should be further explored in the setting of articular cartilage–damaging conditions such as septic arthritis.

In this study, we verified that adjuvant treatment of septic arthritis with local rifampin and NLRP3 inflammasome inhibitors is efficacious. However, our research has some limitations. First, patients with septic arthritis are usually treated with systemic antibiotics twice daily. However, antibiotics were only administered once daily in this study, possibly indicating the use of a subtherapeutic regimen. Future studies will evaluate the effects of twice daily dosing in these models. In addition, the short duration of systemic antibiotic treatment used is not suitable for clinical practice but was evaluated across models because of the significant reduction in MRSA bioburden after only 3 days of treatment. Undetectable MRSA growth was observed in antibiotic-treated groups, complicating the investigation of the efficacy of adjuvant hydrogel therapy. However, when VT-MRSA were developed to investigate the effects of antibiotics on dead bacteria, viable bacteria persisted, potentially in the intracellular compartment, and replicated in broth despite the apparent lack of plated growth for CFU quantification. This both validates the need

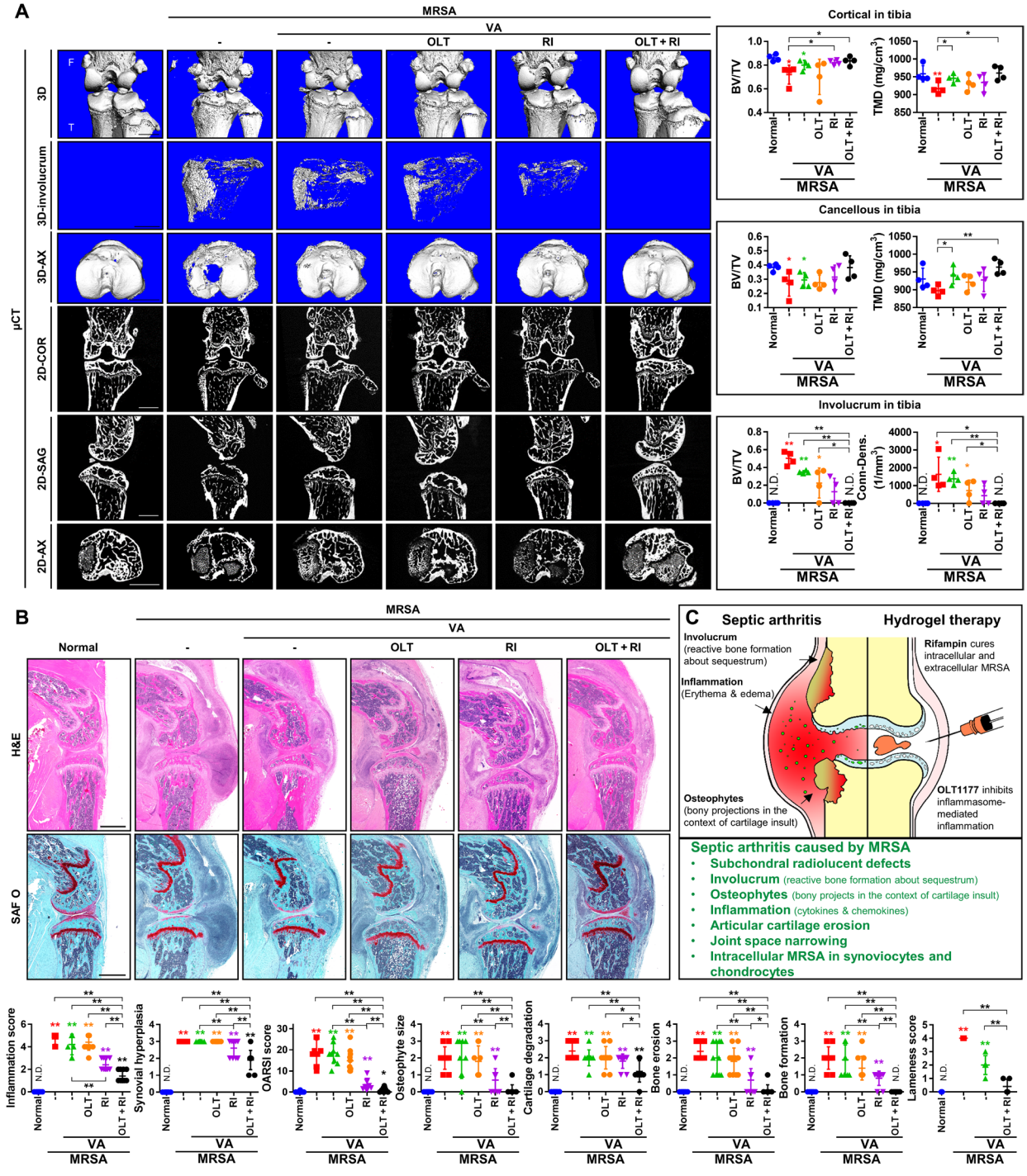

Fig. 6. Local treatment with hydrogels containing rifampin and a NLRP3 inflammasome inhibitor prevents the development of MRSA-induced septic arthritis. C57BL/6 mice were intra-articularly injected under the patella with DPBS (normal) and MRSA (4×10^6 CFU). After a day, vancomycin (30 mg/kg) was administered for 3 days, after which a hydrogel (2%) containing OLT (200 μg per joint), rifampin (RI; 120 μg per joint), and OLT (200 μg per joint) + rifampin (120 μg per joint) ($n = 4$ to 10 per group) was injected intra-articularly under the patella. (**A**) Representative 3D images of the knee and involucrum along the axial plane (AX) and 2D images in the coronal (COR), sagittal (SAG), and axial planes were reconstructed by micro-CT. BV/TV and TMD of cortical and cancellous bone in the tibia were quantified by micro-CT; BV/TV and TMD of cortical and cancellous bone in the femur (fig. S6C). BV/TV and Conn-Dens. of the tibial involucrum were quantified by micro-CT; BV/TV and conn-dens. of involucrum in the femur (fig. S6, A and B). (**B**) Paraffin-embedded tissue sections were stained with H&E and SAF O, from which inflammation score, synovial hyperplasia, OARSI score, osteophyte size, cartilage degradation, bone erosion, and bone formation were calculated and scored (scale bar, 1000 μm). Error bars show means ± SD with individual data points. (**C**) Illustrated summary of the various symptoms of MRSA-induced septic arthritis and the effects of local rifampin and NLRP3 inflammasome inhibitor hydrogel treatment. Error bars show means ± SD with individual data points. One- or two-way ANOVA with Tukey's post hoc analysis was used (*$P < 0.05$ or **$P < 0.01$).

for additional antibiotic therapy, as delivered through the adjuvant, locally applied hydrogel, due to the persistence of bacteria even after exposure to vancomycin. Increased inflammation and cartilage damage were still observed in the presence of these VT bacteria relative to the control and HK conditions.

Together, these findings support our proposed therapeutic concept that concurrent targeting of the NLRP3 inflammasome and bacteria within the intracellular compartment reduced inflammation and obviated permanent cartilage damage. This therapeutic concept may provide an efficient avenue through which to treat bacterial septic arthritis and suggests possible applications to mitigate deleterious inflammatory responses found in other infectious processes.

MATERIALS AND METHODS

Cell culture and antibiotic treatments

The RAW264.7 cell line was purchased from American Type Culture Collection (San Diego, CA, USA) and cultured in high-glucose Dulbecco's modified Eagle's medium (DMEM; Gibco, Grand Island, NY, USA) containing 1% of penicillin/streptomycin solution (Gibco) and 10% of fetal bovine serum (FBS; Gibco). Six to 8-week old female C57BL/6 J mice were purchased from the Jackson laboratory (Bar Harbor, Maine, USA). The femurs were collected from euthanized mice and flushed with minimum essential medium Eagle α (MEMα) complete medium containing 10% of FBS (Gemini Bio, Woodland, CA, USA) and 1% of penicillin/streptomycin solution (Gibco) using a sterile 26-gauge needle. After red blood cell (RBC) lysis using RBC lysis buffer (Invitrogen, Carlsbad, CA, USA), the cells sat overnight in a 10-cm cell culture dish in complete MEMα supplemented with M-CSF (10 ng/ml; Shenandoah Biotechnology, Warwick, PA, USA). All cells were incubated in a humidified atmosphere containing 5% CO_2 at 37°C (Thermo Fisher Scientific Inc., Waltham, MA, USA). Vancomycin hydrochloride was purchased from Sigma-Aldrich Co. (St. Louis, MO, USA). Rifampin was purchased from G-Biosciences (St. Louis, MO, USA). OLT was purchased from the Cayman Chemical Company (Ann Arbor, MI, USA).

MRSA culture and preparation

The USA300-FPR3757 strain of MRSA (*32*) expressive of GFP was provided by A. Prince at Columbia University. Before use, MRSA was kept at −80°C. Bacteria were transferred onto Mueller-Hinton agar plates (Sigma-Aldrich Co., St. Louis, MO, USA) containing oxacillin (6 μg/ml; Sigma-Aldrich Co.) and incubated in a 35°C incubator for 24 hours. GFP fluorescent intensity on the plate was measured using the IVIS Spectrum In Vivo Imaging System (PerkinElmer, Santa Clara, CA, USA). Single MRSA colonies were also planktonically cultured in lysogeny broth (LB; Invitrogen) containing oxacillin (6 μg/ml; Sigma-Aldrich Co.) for 24 hours, after which fluorescence intensity was measured with the ZOE Fluorescent Cell Imager (Bio-Rad Laboratories, Hercules, CA, USA). MRSA (1×10^7 CFU/10 μl) was intra-articularly injected under murine patellae using a U-100 Micro-Fine IV insulin syringe (28-gauge needle; BD Biosciences, San Jose, CA, USA), after which GFP fluorescence intensity was measured using the IVIS Spectrum In Vivo Imaging System (PerkinElmer). MRSA (2×10^9 CFU/ml) was treated with different concentrations of vancomycin (0.625 to 20 mg/ml) for 24 hours to make VT-MRSA and incubated at 65°C for 2 hours to make HK-MRSA. These samples were seeded on a Mueller-Hinton agar plate (Sigma-Aldrich Co.) with or without oxacillin and then incubated in a 35°C incubator for 48 hours; MRSA was used as a positive control. Plate images were measured with the ChemiDoc Touch Imaging System (Bio-Rad Laboratories), and CFU were counted directly.

In vivo animal experiments

All animal experiments were approved by the Yale University Institutional Animal Care and Use Committee (number: 2020-20129). Male C57BL/6 J mice (10 to 14 weeks) were purchased from the Jackson laboratory (Bar Harbor, Maine, USA). Mice were anesthetized with a combination of ketamine (10 mg/ml; Ketaset, Zoetis Inc., MI, USA) and xylazine (1 mg/ml; AnaSed Injection, Akorn Inc., IL, USA). Fur surrounding the knee joint was removed using Veet In Shower Cream (Reckitt Benckiser, Slough, England, UK). Skin overlaying the knee was sterilized with povidone-iodine pads (Professional Disposables International Inc., NY, USA) and isopropyl alcohol pads (Professional Disposables International Inc.). MRSA (0.25×10^6, 1×10^6, and 4×10^6 CFU/10 μl) were intra-articularly injected under the patella using a U-100 Micro-Fine IV Insulin Syringe (28-gauge needle; BD Biosciences); control mice were injected with the same volume of Dulbecco's phosphate-buffered saline (DPBS; Gibco). MRSA (2×10^7 CFU/10 μl), HK-MRSA, and VT-MRSA (20 mg/ml of vancomycin treatment) were intra-articularly injected under the patella using a U-100 Micro-Fine IV Insulin Syringe (28-gauge needle; BD Biosciences); control was injected with the same volume of DPBS (Gibco). After intra-articular injection, the skin overlying the knee joint was sterilized as before. All mice were then placed on a warming pad and monitored until ambulatory.

For vancomycin systemic treatment, vancomycin (30 mg/kg; Sigma-Aldrich Co.) was subcutaneously injected using a U-100 Micro-Fine IV Insulin Syringe (28-gauge needle; BD Biosciences) daily for 3 days after MRSA infection of the knee joint.

For hydrogel local treatment, mice were anesthetized with a combination of ketamine (Zoetis Inc.) and xylazine (Akorn Inc.) and sterilized with povidone-iodine pads (Professional Disposables International Inc.) and isopropyl alcohol pads (Professional Disposables International Inc.). Hydrogel (2%; ESI-BIO, Alameda, CA, USA) containing rifampin (120 μg per joint; G-Biosciences) and/or OLT (200 μg per joint; Cayman Chemical Company) was intra-articularly injected under the patella using a U-100 Micro-Fine IV Insulin Syringe (28-gauge needle; BD Biosciences) after treatment with systemic vancomycin (Sigma-Aldrich Co.). Once again, the skin was sterilized; the mouse was placed on a warming pad and monitored until ambulatory. Lameness was scored on a scale from 0 to 4: 0 = walks normally, 1 = slightly lame when walking, 2 = moderately lame when walking, 3 = severely lame when walking, and 4 = reluctant to walk and not use when walking.

Ex vivo: Human synovial and cartilage tissue experiments

Specimens ($n = 4$) of human synovial and cartilage tissues were collected during knee joint surgery, which was approved by the Institutional Review Board (number: 2000021232) of Yale University. All patients signed an informed consent form for participation in the study and for the use of their biological tissues. Tissues were transferred to a plate containing DMEM and then infected with MRSA (4×10^6 CFU) for 24 hours. Afterward, tissue was allocated for future histologic analysis or RNA isolation or Western blot.

Synovial cells were separated from synovial tissue using collagenase type I (0.25%; STEMCELL Technologies, Vancouver, BC, Canada) and cultured with DMEM (Gibco) containing 1% of penicillin/streptomycin solution (Gibco) and 10% of FBS (Gibco). Passages 3 to 6 of synovial cells were used for future experiments. Synovial cells (1×10^4) were seeded on a 96-well plate (BD Biosciences) and grown overnight in a humidified atmosphere containing 5% CO_2 at 37°C. Synovial cells were treated with OLT (50 to 200 μg/ml) for 1 hour before infection of HK-MRSA (2×10^7 CFU) for 24 hours and then treated with or without ATP (5 mM; Sigma-Aldrich Co.) for 6 hours. Levels of IL-1β (1:2 dilution) and IL-6 (1:100 dilution) were measured using the human IL-1β and IL-6 ELISA Ready-SET-Go! Kit (Invitrogen) according to the manufacturer's instructions. Cytotoxicity was measured by using a CyQUANT LDH Cytotoxicity Assay (Invitrogen) according to the manufacturer's instructions. The levels of IL-1β and lactate dehydrogenase were measured with the BioTek Cytation 5 Cell Imaging Multi-Mode Reader and analyzed using BioTek Gen5 software (BioTek Instruments Inc., Winooski, VT, USA).

In vitro: MRSA infection experiments

RAW264.7 cells (2×10^6) were seeded on a six-well plate (BD Biosciences) and grown overnight in a humidified atmosphere containing 5% CO_2 at 37°C. Single MRSA colonies were planktonically cultured in LB (Invitrogen) containing oxacillin (6 μg/ml; Sigma-Aldrich Co.) for 24 hours. After a day, RAW264.7 cells were infected with MRSA (4×10^6 CFU) for 10, 20, 30, 60, and 120 min. At each time point, culture media was removed, and cells were washed with PBS solution at least three times to eliminate extracellular MRSA.

To analyze intracellular MRSA infection, RAW264.7 cells were fixed in 4% paraformaldehyde (Thermo Fisher Scientific Inc.) for 10 min and stained with Hoechst 33342 (10 mg/ml; Invitrogen) for 10 min before being washed with PBS solution. Immediately afterward, fluorescence was measured using the ZOE Fluorescent Cell Imager (Bio-Rad Laboratories). After infection with MRSA for 120 min, RAW264.7 cells were fixed with 4% paraformaldehyde (Thermo Fisher Scientific Inc.) for 10 min and washed with PBS solution (Gibco). The cells were permeabilized using a 0.2% Triton X-100 solution (Thermo Fisher Scientific Inc.) for 10 min and then blocked with SuperBlock blocking buffer (Thermo Fisher Scientific Inc.) for 30 min; cells were washed with PBS solution (Gibco) at each step. The cells were incubated with Alexa Fluor 488–conjugated phalloidin (Cell Signaling Technology Inc., Danvers, MA, USA, catalog no. 8953) for 1 hour and then stained with Hoechst 33342 (10 mg/ml; Invitrogen) for 10 min, after which they were washed with PBS solution. Fluorescence intensities were detected using the ZOE Fluorescent Cell Imager (Bio-Rad Laboratories).

To investigate bacterial bioburden in CFU from the intracellular compartment, RAW264.7 cells were harvested and then counted with the TC20 Automated Cell Counter (Bio-Rad Laboratories); MRSA expressing GFP in the suspension of RAW264.7 cells were measured by the ZOE Fluorescent Cell Imager (Bio-Rad Laboratories). A total of 1×10^5 cells from the suspension of RAW264.7 cells were plated on Mueller-Hinton agar plates containing oxacillin (6 μg/ml) and incubated for 48 hours. After 2 days, CFU were identified with the ChemiDoc Touch Imaging System (Bio-Rad Laboratories), and CFU was quantified using ImageJ software (National Institutes of Health, Bethesda, MD) (*33*). At each time point, the expression of NLRP3, phosphorylated p38, p38, phosphorylated c-Jun N-terminal kinase (JNK), JNK, phosphorylated extracellular signal–regulated kinase (ERK), ERK, inhibitor of nuclear factor κBα, and β-actin proteins was confirmed by Western blotting.

To gauge the efficacy of various antibiotics against intracellular MRSA, RAW264.7 cells were infected with MRSA (4×10^6 CFU) for 120 min and then treated with vancomycin, rifampin, and vancomycin/rifampin for 1 hour. The plates were washed with PBS solution, after which the RAW264.7 cells were harvested and counted with the TC20 Automated Cell Counter (Bio-Rad Laboratories). A total of 1×10^5 cells from each suspension of RAW264.7 cells were plated on Mueller-Hinton agar plates containing oxacillin (6 μg/ml) and incubated for 48 hours. After 2 days, CFU was detected using the ChemiDoc Touch Imaging System (Bio-Rad Laboratories), and CFU were quantified with ImageJ software (*33*).

RNA-seq and data analysis

Bone marrow isolated from 6- to 8-week-old female C57BL/6 J mice femurs were flushed with MEMα complete medium containing 10% of FBS (Gemini Bio, Woodland, CA, USA) and 1% of penicillin/streptomycin solution (Gibco). The cells sat overnight in a 10-cm cell culture dish in complete MEMα supplemented with M-CSF (10 ng/ml; Shenandoah Biotechnology, Warwick, PA, USA). On the next morning, the floating cells were collected, counted, and seeded in six-well plates at 5×10^5 per well. The cells were cultured for 5 days, and the night before infection, the medium was changed to antibiotic-free medium. During the next day, the cells were left either uninfected or infected with MRSA at a multiplicity of infection of 10 and incubated with MRSA over a period of 24 hours. After the first 2 hours of infection, the medium was changed to MEMα containing gentamicin (50 μg/ml; Sigma-Aldrich Co.). At the end of each time point, the cells were washed twice with PBS, and RNA was harvested using a Qiagen RNeasy mini kit (Qiagen, Germantaown, MD, USA). The quality and quantity of RNA samples were determined using the Agilent bioanalyzer at Columbia Medical Center. RNA (100 ng) was submitted and sequenced by Columbia Genome Center. Briefly, the RNA library was prepared using a TruSeq Stranded mRNA Library Prep kit (Illumina, San Diego, CA, USA), and Index Adapters were added using a TruSeq RNA Single Indexes Set A kit (Illumina). The libraries were then mixed with a NextSeq 500 v2.5 reagent kit and sequenced in an Illumina's NextSeq 500 sequencer. RNA-seq data are deposited in Sequence Read Archive (SRA) under the National Center for Biotechnology Information (accession number: PRJNA647064). Differentially expressed genes in MRSA infection were compared to the noninfectious conditions and defined as genes with a fold change ≥ 2 or ≤ -2, and with a Benjamini-Hochberg–adjusted P value of <0.05. The pathways, upstream factors, and biologic function of genes increased by MRSA infection were analyzed by Ingenuity Pathway Analysis (Qiagen Bioinformatics).

CBC analysis

Whole blood was collected via cardiac puncture using a 1-ml BD slip-tip disposable tuberculin syringe (28-gauge needle; BD Biosciences) and immediately mixed with a 0.5 M EDTA (pH 8.0) solution (1:10 ratio; AmericanBio, Natick, MA, USA). CBC analysis, including WBC count, lymphocyte percentage, monocyte percentage, neutrophil percentage, RBC count, and platelet count, was performed using the Abaxis VetScan HM5 Hematology System

(Abaxis North America, Union City, CA, USA) according to the manufacturer's instructions.

MPO activity analysis

To investigate MPO activity, mice were intraperitoneally injected with the XenoLight RediJect Chemiluminescent Inflammation Probe (PerkinElmer, catalog no. 760536) according to the manufacturer's instructions. Luminescence intensity was measured and analyzed using the IVIS Spectrum In Vivo Imaging System (PerkinElmer).

Synovial fluid analysis

DPBS (10 μl) was intra-articularly injected under murine patellae using a U-100 Micro-Fine IV Insulin Syringe (28-gauge needle; BD Biosciences), aspirated, and transferred to a sterile tube. Synovial fluid cell number (1:10 dilution) was measured using the TC20 Automated Cell Counter (Bio-Rad Laboratories). The presence of GFP-labeled MRSA within synovial cells was confirmed using the ZOE Fluorescent Cell Imager (Bio-Rad Laboratories). A total of 1×10^4 cells from the synovial fluid were plated on Mueller-Hinton agar plates containing oxacillin (6 μg/ml) for 48 hours, after which the plate image was detected by the ChemiDoc Touch Imaging System (Bio-Rad Laboratories). CFU were then counted directly. The levels of IL-6 and IL-1β in synovial fluid (1:100 dilution) were measured using the IL-6 and IL-1β ELISA Ready-SET-Go! Kit (Invitrogen) according to the manufacturer's instructions. The levels of IL-6 and IL-1β were measured with the BioTek Cytation 5 Cell Imaging Multi-Mode Reader and analyzed using BioTek Gen5 software (BioTek Instruments Inc., Winooski, VT, USA). Whole proteins were isolated from synovial cells with or without vancomycin treatment after MRSA infection as detailed below via Western blotting. When the control was pulled down, this was not performed because enough protein could not be extracted for Western blotting. Cytokine expression was subsequently confirmed by multiplex cytokine/chemokine analysis.

RNA extraction and real-time polymerase chain reaction analysis

Total RNA from human and mouse tissues were extracted using the GE Healthcare Illustra RNAspin Mini Isolation Kit (GE Healthcare, Madison, WI, USA) according to the manufacturer's instructions, and RNA concentrations were measured with the NanoDrop 2000c Spectrophotometer (Thermo Fisher Scientific Inc.). Afterward, complementary DNA was synthesized using the ReverTra Ace™ qPCR RT Master Mix (Toyobo, Osaka, Japan) according to the manufacturer's instructions. Gene expression patterns were measured via real-time polymerase chain reaction using Thunderbird SYBR qPCR Mix (Toyobo) alongside one of multiple specific primer sequences (fig. S12) according to the manufacturer's instructions. Reactions were performed using a 96-well plate using the StepOnePlus Real-Time PCR System (Applied Biosystems, Foster City, CA, USA), with a 40-cycle profile. Relative expression levels were normalized with *GAPDH* using the $2^{-\Delta\Delta Ct}$. Principal components analysis (PCA) was applied to each case of the groups and measured by QStudioMetrics (https://github.com/gmrandazzo/QStudioMetrics).

Immunohistochemistry analysis

Immunohistochemistry (IHC) was conducted using a Rabbit-Specific HRP/DAB Detection IHC Detection Kit–Micro-polymer (Abcam, Cambridge, MA, USA, catalog no. ab236469). Slides were first deparaffinized by washing them three times in xylene (Thermo Fisher Scientific Inc.) for 5 min and in graded ethanol (Decon Laboratories Inc., PA, USA) concentrations—100, 95, and 70%—for 5 min each. Antigen unmasking was performed using a heated 0.1 M sodium citrate solution (J. T. Baker, NJ, USA) for 10 min. Following antigen unmasking, slides were washed in tris-buffered saline with Tween® 20 (TBST) solution (Affymetrix, Santa Clara, CA, USA) three times for 5 min each. Hydrogen peroxide blocking was performed for 30 min using the IHC detection kit at room temperature. Slides were then washed in TBST solution three times for 5 min each. Sections were then incubated with protein block from the kit for 30 min and then incubated with the primary antibodies for NLRP3 (AdipoGen, San Diego, CA, USA, catalog no. AG-20B-0014-C100), IL-1β (Abcam, catalog no. ab9722), and MMP3 (Abcam, catalog no. ab52915) at a concentration of 1:200 overnight at 4°C. After overnight incubation, slides were washed in TBST solution three times for 5 min each. IHC was performed by applying a goat anti-rabbit horseradish peroxidase (HRP) conjugate for 30 min. Slides were washed in TBST solution afterward. Samples were then visualized by diaminobenzidine (DAB) substrate. DAB-visualized sections were then counterstained with Harris' hematoxylin, 1% acid alcohol, and ammonium water. Following counterstaining, the tissues were rehydrated in 100% ethanol three times for 5 min and xylene three times for 5 min before coverslips were applied. Slides were photographed using the BioTek Cytation 5 Cell Imaging Multi-Mode Reader and then analyzed by BioTek Gen5 software (Bio-Tek Instruments Inc.). Positive cells were counted using QuPath software (Queen's University Belfast, Belfast, Northern Ireland, UK) (*34*).

Histological evaluation

Resected knee joint tissues from human patients were fixed with PROTOCOL 10% Buffered Formalin (Thermo Fisher Scientific Inc.) and decalcified with 10% EDTA solution (Sigma-Aldrich Co.) for 3 weeks at 4°C. Paraffin-embedded tissue sections were stained with H&E, SAF O, and TRAP according to the manufacturer's instructions. Images of the stained knee joint tissues were captured with the BioTek Cytation 5 Cell Imaging Multi-Mode Reader and analyzed by BioTek Gen5 software (Bio-Tek Instruments Inc.). The H&E-stained images were used for inflammation scoring and to determine synovial hyperplasia. Inflammation was scored 0 to 5: 0 = normal, 1 = minimal infiltration of inflammatory cells, 2 = mild infiltration of inflammatory cells, 3 = moderate infiltration of inflammatory cells with moderate edema, 4 = marked infiltration of inflammatory cells with marked edema, and 5 = severe infiltration of inflammatory cells with severe edema. Synovial hyperplasia was scored 0 to 3 according to the following standard: 0 = normal; 1 = mild, two to three cells thick; 2 = moderate, four to five cells thick; and 3 = severe, >6 cells thick. The number of cells in the synovial capsule were measured and counted on H&E-stained images using QuPath software (*34*). SAF O–stained images were used to generate OARSI scores and characterize osteophyte size, cartilage degradation, bone erosion, and bone formation. OARSI scoring was scored according to OARSI guidelines (*35*). Osteophyte size was scored from 0 to 3 according to the following standard: 0 = normal; 1 = small, approximately the same thickness as the adjacent cartilage; 2 = medium, one to three times the thickness of the adjacent cartilage; and 3 = large, >3 times the thickness of the adjacent

cartilage. Cartilage degradation was scored from 0 to 3 according to the following standard: 0 = normal; 1 = mild, loss of proteoglycan staining in the superficial layer; 2 = moderate, moderate loss of proteoglycan staining; and 3 = severe, complete loss of proteoglycan staining. Bone erosion was scored 0 to 3 according to the following standard: 0 = normal; 1 = mild, loss of bone at a few sites; 2 = moderate, loss of bone at some sites; and 3 = severe, loss of bone at many sites. Bone formation was scored 0 to 3 according to the following standard: 0 = normal; 1 = small, approximately the same thickness as the adjacent cartilage; 2 = medium, one to three times the thickness of the adjacent cartilage; and 3 = large, >3 times the thickness of the adjacent cartilage. Cartilage thickness was measured on SAF O–stained images by averaging five regions of articular cartilage under the staining regions using ImageJ software (*33*). Chondrocyte numbers in the articular cartilage from SAF O–stained images were measured and counted using QuPath software (*34*). TRAP-positive cells were measured and counted using QuPath software (*34*). All histological evaluations were carried out blinded by two separate investigators.

Multiplex IHC analysis

Slides were first deparaffinized by washing them thrice in xylene (Thermo Fisher Scientific Inc.) for 5 min and in graded ethanol (Decon Laboratories Inc., Pittsburg, PA, USA)—100, 95, and 70%—for 5 min each. Antigen unmasking was performed using a heated SignalStain Citrate Unmasking Solution (Cell Signaling Technology Inc., catalog no. #14746) for 10 min. Following antigen unmasking, slides were washed in TBST solution (Affymetrix) three times for 5 min each. Hydrogen peroxide (10%) was made with 20 ml of 30% hydrogen peroxide aqueous solution (J.T. Baker, Phillipsburg, NJ, USA) and 180 ml of methanol (J.T. Baker) and was applied to each slide for 30 min at room temperature. Slides were then washed in TBST solution three times for 5 min each. Sections were then incubated with Animal-Free Blocking Solution (Cell Signaling Technology Inc., catalog no. #15019) for 30 min and incubated with the desired primary antibody at a 1:200 dilution for 60 min. After primary antibody incubation, slides were washed in TBST solution three times for 5 min each. Depending on primary antibody, slides were treated with either SignalStain Boost IHC Detection Reagent (HRP, Rabbit)/SignalStain Boost IHC Detection Reagent (HRP, Mouse) for 30 min. Slides were washed in TBST solution three times for 5 min. After incubating in secondary antibody, slides were washed in TBST solution three times for 5 min. Slides were then treated for 10 min with either the TSA Plus Fluorescein System (PerkinElmer, catalog no. NEL741B001KT) or the TSA Plus Cyanine 5 System (PerkinElmer, catalog no. NEL741B001KT). The selected fluorescent dye underwent a 1:50 dilution in Plus Amplification Diluent (PerkinElmer, catalog no. FP1135). Next, the slides were washed in TBST solution three times for 5 min while avoiding light exposure. Afterward, slides were incubated in SignalStain Citrate Unmasking Solution for 20 min. After incubation with citrate, slides were incubated with the next selected primary antibody for 60 min. Slides were washed in TBST solution three times for 5 min while limiting light exposure. Then, slides were incubated for 30 min in either SignalStain Boost IHC Detection HRP, Rabbit (Cell Signaling Technology Inc., catalog no. #8114) or SignalStain Boost IHC Detection HRP, Mouse (Cell Signaling Technology Inc., catalog no. #8125) depending on the specific primary antibody. Slides were washed in TBST solution three times for 5 min while limiting light exposure. Slides were then incubated for 10 min in either TSA Plus Fluorescein System (Perkin Elmer) or TSA Plus Cyanine 5 System (Perkin Elmer). The selected fluorescent dye was diluted at 1:50 in Plus Amplification Diluent (Perkin Elmer) and then washed in TBST solution three times for 5 min while limiting light exposure. Last, slides were coverslipped using VECTASHIELD Mounting Medium with DAPI (Vector Laboratories Inc., Burlingame, CA, USA, catalog no. H-1200). Fluorescent activity was detected using LSM 780 confocal microscopy (Carl Zeiss, Jena, Germany, LSM 780 model) and analyzed by Zen 2010 software (Carl Zeiss).

Multiplex cytokine/chemokine analysis

The concentrations of various cytokines, chemokines, and other factors in serum and synovial fluid were measured by MILLIPLEX MAP Mouse Cytokine/Chemokine Magnetic Bead Panel-Immunology Multiplex Assay from Millipore (Billerica, MA, USA) according to the manufacturer's instructions. Serum and synovial fluid were incubated with 100 μg of vancomycin for 30 min; the TV of the solution was then volume-adjusted with assay buffer. A 96-well filter plate was loaded with either 50 μl of a prepared standard solution or 50 μl of serum and synovial fluid. The solutions in the plate were then incubated with capture antibody–conjugated beads at ±800 rpm for 30 min, at room temperature, and in the dark. Wells were vacuum-aspirated and washed with 100 μl of wash buffer three times. Samples were incubated with 25 μl of biotinylated detection antibody at ±800 rpm for 30 min, at room temperature, and in the dark. After three more washes, 50 μl of streptavidin-phycoerythrin was added to each well and incubated for 10 min at ±800 rpm at room temperature and in the dark. After one final wash, the beads were resuspended in 125 μl of sheath buffer for measurement with the Luminex 200 (Luminex, Austin, TX, USA). PCA was performed with QStudioMetrics (https://github.com/gmrandazzo/QStudioMetrics).

Protein isolation and Western blot analysis

Extraction of whole protein from tissue was performed using the Tissue Protein Extraction Reagent (Thermo Fisher Scientific Inc.), while extraction of whole cellular protein was performed using the Mammalian Protein Extraction Reagent (Thermo Fisher Scientific Inc.). Protein concentrations were obtained using a bicinchoninic acid protein assay kit (Thermo Fisher Scientific Inc.) following the manufacturer's protocol. Protein samples were then prepared with 4× Laemmli protein sample buffer (Bio-Rad Laboratories) according to the manufacturer's instructions. Using the Mini-PROTEAN Tetra Cell and Mini Trans-Blot electrophoretic transfer cell system, protein separation and transfer were accomplished using a 4 to 20% SDS–polyacrylamide gel electrophoresis gel (Bio-Rad Laboratories) and polyvinylidene difluoride membrane (Bio-Rad Laboratories), respectively. Membranes were washed using TBST solution (Affymetrix, Santa Clara, CA, USA) and then blocked using 2% bovine serum albumin (Sigma-Aldrich Co.) in TBST solution for 1 hour. They were then immunoblotted with primary antibodies, including PARP1 (Cell Signaling Technology Inc., catalog no. #9532), caspase-3 (Cell Signaling Technology Inc., catalog no. #9662), Bcl2 (Cell Signaling Technology Inc., catalog no. #2870), NLRP3 (Adipogen, catalog no. AG-20B-0014-C100), IL-1β (Cell Signaling Technology Inc., catalog no. #12426 or #12703), caspase-1 (Adipogen, catalog no. AG-20B-0042), ASC (Cell Signaling Technology Inc., catalog

no. #67824 or Santa Cruz Biotechnology, Santa Cruz, CA, USA, catalog no. SC-514414), MMP3 (Abcam, catalog no. ab52915), cathepsin K (Abcam, catalog no. ab19027), GSDME (Abcam, catalog no. ab215191), GSDME (Abcam, catalog no. ab209845), and β-actin (Cell Signaling Technology Inc., catalog no. #3700) and left on a shaker at 4°C overnight. The following day, the membranes were washed using TBST solution and then treated with HRP-conjugated anti-mouse or anti-rabbit immunoglobulin G antibody (Cell Signaling Technology Inc.) for 1 hour. Membranes were washed using TBST solution before the expression levels of proteins were detected by the ChemiDoc Touch Imaging System (Bio-Rad Laboratories) while using a SuperSignal™ West Pico PLUS Chemiluminescent Substrate and/or the SuperSignal West Femto Maximum Sensitivity Substrate (Thermo Fisher Scientific Inc.). Band intensities were measured with ImageJ software (*33*) and normalized to β-actin expression levels.

Hydrogel experiments

Rifampin (600 μg) was mixed with three different percentages of HyStem Hydrogel (0.5, 1, and 2%; ESI-BIO, Alameda, CA, USA) and then applied to polyester (PET) track-etched membrane inserts (3.0-μm pore size; Corning Incorporated Life Science, NY, USA) for 30 min in a biosafety cabinet. Afterward, inserts were transferred into 24-well plates with DMEM containing 10% FBS and 1% of a penicillin/streptomycin solution (Gibco) and then incubated in a humidified atmosphere containing 5% CO_2 at 37°C (Thermo Fisher Scientific Inc.). Kinetic cumulative release of rifampin (absorbance = 336 nm) was measured by the NanoDrop 2000c Spectrophotometer (Thermo Fisher Scientific Inc.). Media containing rifampin (600 μg) was used as a positive control (100%). On days 1, 4, and 7, we washed the inserts with PBS solution at least three times and transferred them into LB media containing oxacillin (6 μg/ml) and MRSA (4×10^6 CFU). The inserts were then incubated for 24 hours. MRSA proliferation was measured by the NanoDrop 2000c Spectrophotometer at an absorbance level of 600 nm (Thermo Fisher Scientific Inc.) using cuvettes. LB media (100 μl) with or without rifampin hydrogel at a dilution of $1{:}10^5$ were seeded on Mueller-Hinton agar plates containing oxacillin (6 μg/ml) for 48 hours, after which CFU numbers were counted using ImageJ software (*33*).

Disk diffusion assay and antibacterial absorbance assay

A single MRSA colony was planktonically cultured in LB (Invitrogen) media containing oxacillin (6 μg/ml; Sigma-Aldrich Co.) for 24 hours, spread on Mueller-Hinton agar plates (Sigma-Aldrich Co.) containing oxacillin (6 μg/ml) using a sterile cotton-tipped applicator (McKesson Medical, San Francisco, CA, USA), and grown for 1 hour. Different concentrations of vancomycin, rifampin, and vancomycin/rifampin were prepared, and 20 μl of each solution was loaded onto sterile blank paper discs (6 mm; BD Biosciences) and dried for 1 hour. The dried discs were transferred to a Mueller-Hinton agar plate containing oxacillin (6 μg/ml) and MRSA and then incubated for 24 hours. After a day, the diameter of each inhibition zone was measured using a digital electronic caliper (Fine Science Tools, Heidelberg, Germany), and images were captured with the ChemiDoc Touch Imaging System (Bio-Rad Laboratories). For the antibacterial absorbance assay, MRSA (4×10^6 CFU) were seeded into LB (Invitrogen) media containing oxacillin (6 μg/ml; Sigma-Aldrich Co.) and incubated at 35°C. After 2 hours, we treated the LB media with three different concentrations of vancomycin (50 to 200 μg) or rifampin (75 to 300 ng). MRSA growth was measured by absorbance at 600 nm using the NanoDrop 2000c Spectrophotometer (Thermo Fisher Scientific Inc.) at 1-hour intervals for a total of 7 hours.

Micro-CT analysis

Knee joint tissues were fixed with PROTOCOL 10% Buffered Formalin (Thermo Fisher Scientific Inc.) for 5 days, transferred to 70% ethanol (Thermo Fisher Scientific Inc.), and stored at 4°C. Sections of murine knee joints measuring 10.9 mm were used to perform femoral and tibial condyle micro-CT analyses using a Scanco μCT 50 (Scanco Medical, Brüttisellen, Switzerland) system. Samples were immersed in 70% ethanol, and the following settings were used to acquire each image: 6-μm voxel size, 55KVp, 0.36° rotation step (180° angular range), and 1300-ms exposure per view. Then, Scanco μCT software (DECwindows Motif 1.6; Hewlett-Packard) was used for 3D reconstruction of images. After 3D reconstruction, volumes were segmented using a global threshold of 400 mg HA/cm^3. TMD, directly measured TV, BV, BV fraction (BV/TV), Conn-Dens., surface-to-volume ratio (BS/BV), thickness (Tb.Th), number (Tb.N), and separation (Tb.Sp) were calculated for both trabecular and ectopic bone. Apparent density, TMD, BV/TV, bone thickness, BS/BV, total area (TA), bone area (BA), and BA-to-TA ratio (BA/TA) were calculated for condyle cortices.

Statistical analysis

All experimental data were analyzed using one- and two-way analysis of variance (ANOVA) in GraphPad Prism version 8 (GraphPad Software Inc., La Jolla, CA, USA).

SUPPLEMENTARY MATERIALS

Supplementary material for this article is available at http://advances.sciencemag.org/cgi/content/full/7/26/eabf2665/DC1

View/request a protocol for this paper from *Bio-protocol*.

REFERENCES AND NOTES

1. M. E. Shirtliff, J. T. Mader, Acute septic arthritis. *Clin. Microbiol. Rev.* **15**, 527–544 (2002).
2. C. J. Mathews, V. C. Weston, A. Jones, M. Field, G. Coakley, Bacterial septic arthritis in adults. *Lancet* **375**, 846–855 (2010).
3. K. D. Alder, I. Lee, A. M. Munger, H.-K. Kwon, M. T. Morris, S. V. Cahill, J. Back, K. E. Yu, F. Y. Lee, Intracellular *Staphylococcus aureus* in bone and joint infections: A mechanism of disease recurrence, inflammation, and bone and cartilage destruction. *Bone* , 115568 (2020).
4. K. Oikonomopoulou, E. P. Diamandis, M. D. Hollenberg, V. Chandran, Proteinases and their receptors in inflammatory arthritis: An overview. *Nat. Rev. Rheumatol.* **14**, 170–180 (2018).
5. J. J. Dubost, M. Soubrier, C. De Champs, J. M. Ristori, J. L. Bussiere, B. Sauvezie, No changes in the distribution of organisms responsible for septic arthritis over a 20 year period. *Ann. Rheum. Dis.* **61**, 267–269 (2002).
6. J. G. Hunter, J. M. Gross, J. D. Dahl, S. L. Amsdell, J. T. Gorczyca, Risk factors for failure of a single surgical debridement in adults with acute septic arthritis. *J. Bone Joint Surg. Am.* **97**, 558–564 (2015).
7. S. R. Arnold, D. Elias, S. C. Buckingham, E. D. Thomas, E. Novais, A. Arkader, C. Howard, Changing patterns of acute hematogenous osteomyelitis and septic arthritis: Emergence of community-associated methicillin-resistant *Staphylococcus aureus*. *J. Pediatr. Orthop.* **26**, 703–708 (2006).
8. A. Moldovan, M. J. Fraunholz, In or out: Phagosomal escape of *Staphylococcus aureus*. *Cell. Microbiol.* **21**, e12997 (2019).
9. S. L. Brandt, N. E. Putnam, J. E. Cassat, C. H. Serezani, Innate immunity to *Staphylococcus aureus*: Evolving paradigms in soft tissue and invasive infections. *J. Immunol.* **200**, 3871–3880 (2018).
10. J. Josse, F. Velard, S. C. Gangloff, *Staphylococcus aureus* vs. Osteoblast: Relationship and consequences in osteomyelitis. *Front. Cell. Infect. Microbiol.* **5**, 85 (2015).
11. K. Yu, L. Song, H. P. Kang, H.-K. Kwon, J. Back, F. Y. Lee, Recalcitrant methicillin-resistant *Staphylococcus aureus* infection of bone cells: Intracellular penetration and control strategies. *Bone Joint Res.* **9**, 49–59 (2020).

12. S. Bongers, P. Hellebrekers, L. P. H. Leenen, L. Koenderman, F. Hietbrink, Intracellular penetration and effects of antibiotics on *Staphylococcus aureus* inside human neutrophils: A comprehensive review. *Antibiotics* **8**, 54 (2019).
13. S. V. Cahill, H. K. Kwon, J. Back, I. Lee, S. Lee, K. D. Alder, Z. Hao, K. E. Yu, C. M. Dussik, T. R. Kyriakides, F. Y. Lee, Locally delivered adjuvant biofilm-penetrating antibiotics rescue impaired endochondral fracture healing caused by MRSA infection. *J. Orthop. Res.* **39**, 402–414 (2021).
14. C. A. Dinarello, The IL-1 family of cytokines and receptors in rheumatic diseases. *Nat. Rev. Rheumatol.* **15**, 612–632 (2019).
15. K. V. Swanson, M. Deng, J. P. Ting, The NLRP3 inflammasome: Molecular activation and regulation to therapeutics. *Nat. Rev. Immunol.* **19**, 477–489 (2019).
16. R. Nair, M. L. Schweizer, N. Singh, Septic arthritis and prosthetic joint infections in older adults. *Infect. Dis. Clin. North Am.* **31**, 715–729 (2017).
17. J.-Y. Seo, C.-H. Suh, J.-Y. Jung, A.-R. Kim, J. W. Yang, H.-A. Kim, The neutrophil-to-lymphocyte ratio could be a good diagnostic marker and predictor of relapse in patients with adult-onset Still's disease: A STROBE-compliant retrospective observational analysis. *Medicine* **96**, e7546 (2017).
18. A. Swan, H. Amer, P. Dieppe, The value of synovial fluid assays in the diagnosis of joint disease: A literature survey. *Ann. Rheum. Dis.* **61**, 493–498 (2002).
19. C. Marchetti, B. Swartzwelter, F. Gamboni, C. P. Neff, K. Richter, T. Azam, S. Carta, I. Tengesdal, T. Nemkov, A. D'Alessandro, C. Henry, G. S. Jones, S. A. Goodrich, J. P. S. Laurent, T. M. Jones, C. L. Scribner, R. B. Barrow, R. D. Altman, D. B. Skouras, M. Gattorno, V. Grau, S. Janciauskiene, A. Rubartelli, L. A. B. Joosten, C. A. Dinarello, OLT1177, a β-sulfonyl nitrile compound, safe in humans, inhibits the NLRP3 inflammasome and reverses the metabolic cost of inflammation. *Proc. Natl. Acad. Sci. U.S.A.* **115**, E1530–E1539 (2018).
20. M. Rashidi, I. P. Wicks, J. E. Vince, Inflammasomes and cell death: Common pathways in microparticle diseases. *Trends Mol. Med.* **26**, 1003–1020 (2020).
21. C. Liu, A. Bayer, S. E. Cosgrove, R. S. Daum, S. K. Fridkin, R. J. Gorwitz, S. L. Kaplan, A. W. Karchmer, D. P. Levine, B. E. Murray, M. J. Rybak, D. A. Talan, H. F. Chambers, Clinical practice guidelines by the infectious diseases society of america for the treatment of methicillin-resistant *Staphylococcus aureus* infections in adults and children: Executive summary. *Clin. Infect. Dis.* **52**, 285–292 (2011).
22. J.-A. Paiva, P. Eggimann, Treatment of severe MRSA infections: Current practice and further development. *Intensive Care Med.* **43**, 233–236 (2017).
23. J. Y. Li, D. J. Mooney, Designing hydrogels for controlled drug delivery. *Nat. Rev. Mater.* **1**, 16071 (2016).
24. H. D. Gresham, J. H. Lowrance, T. E. Caver, B. S. Wilson, A. L. Cheung, F. P. Lindberg, Survival of *Staphylococcus aureus* inside neutrophils contributes to infection. *J. Immunol.* **164**, 3713–3722 (2000).
25. M. Kubica, K. Guzik, J. Koziel, M. Zarebski, W. Richter, B. Gajkowska, A. Golda, A. Maciag-Gudowska, K. Brix, L. Shaw, T. Foster, J. Potempa, A potential new pathway for *Staphylococcus aureus* dissemination: The silent survival of *S. aureus* phagocytosed by human monocyte-derived macrophages. *PLOS ONE* **3**, e1409 (2008).
26. J. K. Ellington, M. Harris, M. C. Hudson, S. Vishin, L. X. Webb, R. Sherertz, Intracellular *Staphylococcus aureus* and antibiotic resistance: Implications for treatment of staphylococcal osteomyelitis. *J. Orthop. Res.* **24**, 87–93 (2006).
27. D. Yang, A. R. Wijenayaka, L. B. Solomon, S. M. Pederson, D. M. Findlay, S. P. Kidd, G. J. Atkins, Novel insights into *Staphylococcus aureus* deep bone infections: The involvement of osteocytes. *MBio* **9**, e00415-18 (2018).
28. B. C. Kahl, K. Becker, B. Loffler, Clinical significance and pathogenesis of Staphylococcal small colony variants in persistent infections. *Clin. Microbiol. Rev.* **29**, 401–427 (2016).
29. E. A. Masters, R. P. Trombetta, K. L. de Mesy Bentley, B. F. Boyce, A. L. Gill, S. R. Gill, K. Nishitani, M. Ishikawa, Y. Morita, H. Ito, S. N. Bello-Irizarry, M. Ninomiya, J. D. Brodell Jr., C. C. Lee, S. P. Hao, I. Oh, C. Xie, H. A. Awad, J. L. Daiss, J. R. Owen, S. L. Kates, E. M. Schwarz, G. Muthukrishnan, Evolving concepts in bone infection: Redefining "biofilm", "acute vs. chronic osteomyelitis", "the immune proteome" and "local antibiotic therapy". *Bone Res* **7**, 20 (2019).
30. J. Perlroth, M. Kuo, J. Tan, A. S. Bayer, L. G. Miller, Adjunctive use of rifampin for the treatment of *Staphylococcus aureus* infections: A systematic review of the literature. *Arch. Intern. Med.* **168**, 805–819 (2008).
31. P. Birmingham, J. M. Helm, P. A. Manner, R. S. Tuan, Simulated joint infection assessment by rapid detection of live bacteria with real-time reverse transcription polymerase chain reaction. *J. Bone Joint Surg. Am.* **90**, 602–608 (2008).
32. B. A. Diep, S. R. Gill, R. F. Chang, T. H. Phan, J. H. Chen, M. G. Davidson, F. Lin, J. Lin, H. A. Carleton, E. F. Mongodin, G. F. Sensabaugh, F. Perdreau-Remington, Complete genome sequence of USA300, an epidemic clone of community-acquired meticillin-resistant *Staphylococcus aureus*. *Lancet* **367**, 731–739 (2006).
33. C. A. Schneider, W. S. Rasband, K. W. Eliceiri, NIH Image to ImageJ: 25 years of image analysis. *Nat. Methods* **9**, 671–675 (2012).
34. P. Bankhead, M. B. Loughrey, J. A. Fernandez, Y. Dombrowski, D. G. McArt, P. D. Dunne, S. McQuaid, R. T. Gray, L. J. Murray, H. G. Coleman, J. A. James, M. Salto-Tellez, P. W. Hamilton, QuPath: Open source software for digital pathology image analysis. *Sci. Rep.* **7**, 16878 (2017).
35. K. P. Pritzker, S. Gay, S. A. Jimenez, K. Ostergaard, J.-P. Pelletier, P. A. Revell, D. Salter, W. B. van den Berg, Osteoarthritis cartilage histopathology: Grading and staging. *Osteoarthr. Cartil.* **14**, 13–29 (2006).

Acknowledgments: We appreciate the histologic assistance of N. Troiano and J. Fretz, Department of Orthopaedics and Rehabilitation, Yale School of Medicine). **Funding:** This research was supported by National Institutes of Health (NIH) National Institute of Arthritis and Musculoskeletal and Skin Diseases (NIAMS) grants AR056246 and AR068353. **Author contributions:** H.-K.K. designed and performed experiments and analyzed the data. F.Y.L. conceived and designed the overall study as the principal investigator. K.E.Y., C.M.D., S.V.C., K.D.A., I.L., J.B., and S.L. performed the experiments. I.L., S.L., K.E.Y., C.M.D., and S.V.C. performed and analyzed histology. J.C. contributed to bacterial research design and data analysis. L.S. performed and constructed the RNA-seq. T.R.K. contributed to hydrogel research design and data analysis. All authors contributed to the writing and editing of the manuscript and approved the final manuscript. **Competing interests:** The authors declare that they have no competing interests. **Data and materials availability:** All data needed to evaluate the conclusions in the paper are present in the paper and/or the Supplementary Materials. Additional data related to this paper may be requested from the authors.

Submitted 14 October 2020
Accepted 12 May 2021
Published 25 June 2021
10.1126/sciadv.abf2665

Citation: H.-K. Kwon, I. Lee, K. E. Yu, S. V. Cahill, K. D. Alder, S. Lee, C. M. Dussik, J. Back, J. Choi, L. Song, T. R. Kyriakides, F. Y. Lee, Dual therapeutic targeting of intra-articular inflammation and intracellular bacteria enhances chondroprotection in septic arthritis. *Sci. Adv.* **7**, eabf2665 (2021).